RDA-TR-9000-001

LINEAR AND NON-LINEAR EMP DIFFUSION THROUGH A FERROMAGNETIC CONDUCTING SLAB

JULY 1975

By:
W.J. KARZAS
C.T.C. MO

This research was conducted under the Office of Naval Research, Contract No. N00014-75-C-0104, Task No. NR 321-046, and was funded by the Naval Electronic Systems Command.

R & D ASSOCIATES
Post Office Box 9695
Marina del Rey,
California 90291

4640 ADMIRALTY WAY • MARINA DEL REY • TELEPHONE: (213) 822-1715

REPORT DOCUMENTATION PAGE

READ INSTRUCTIONS BEFORE COMPLETING FORM

1. REPORT NUMBER: RDA-TR-9000-001	2. GOVT ACCESSION NO.
3. RECIPIENT'S CATALOG NUMBER	
4. TITLE (and Subtitle): LINEAR AND NON-LINEAR EMP DIFFUSION THROUGH A FERROMAGNETIC CONDUCTING SLAB	5. TYPE OF REPORT & PERIOD COVERED: Special Technical Report
	6. PERFORMING ORG. REPORT NUMBER: RDA-TR-9000-001
7. AUTHOR(s): William J. Karzas, Charles T. C. Mo	8. CONTRACT OR GRANT NUMBER(s): N00014-75-C-0104
9. PERFORMING ORGANIZATION NAME AND ADDRESS: R & D Associates, 4640 Admiralty Way, Marina del Rey, California 90291	10. PROGRAM ELEMENT, PROJECT, TASK AREA & WORK UNIT NUMBERS: NR 321-046
11. CONTROLLING OFFICE NAME AND ADDRESS: Office of Naval Research, Department of the Navy, Arlington, Virginia 22217	12. REPORT DATE: July 1975
	13. NUMBER OF PAGES: 71
14. MONITORING AGENCY NAME & ADDRESS (if different from Controlling Office)	15. SECURITY CLASS. (of this report): UNCLASSIFIED
	15a. DECLASSIFICATION DOWNGRADING SCHEDULE

16. DISTRIBUTION STATEMENT (of this Report)

Cleared for public release and sale; distribution unlimited.

17. DISTRIBUTION STATEMENT (of the abstract entered in Block 20, if different from Report)

18. SUPPLEMENTARY NOTES

Research conducted under Office of Naval Research Contract No. N00014-75-C-0104; Task No. NR 321-046. Funded by Naval Electronic Systems Command.

19. KEY WORDS (Continue on reverse side if necessary and identify by block number)

EMP; diffusion; penetration; shielding.

20. ABSTRACT (Continue on reverse side if necessary and identify by block number)

The penetration of an EMP field, such as a plane wave incident upon and a surge arrestor current terminated at a shielding plate, through a ferromagnetic conducting slab made of iron or steel is investigated. The diffusion of the electromagnetic field in the highly conducting slab is complicated by the presence of the nonlinear saturation of the ferromagnetic permeability μ, due to the large amplitude of the incident EMP. Such a saturation, compared to the no-saturation constant μ case, makes the field diffuse faster

DD FORM 1 JAN 73 1473 EDITION OF 1 NOV 65 IS OBSOLETE

19. KEY WORDS (Continued)

20. ABSTRACT (Continued)

in the slab and admits a stronger penetrated field inside the shielding if the slab is thin and the pulse duration is long, as expected. On the contrary, if the slab is thick and the pulse width is short, as the practical cases are, the saturation reduces the penetrated field but maintains its time shape. In this report, first we solve analytically the one-dimension plane wave incidence problem for a slab with a constant μ. Then we use the results to partly predict and to interpret the numerical values obtained by using a finite difference code for the case of a nonlinear μ. These comparisons reveal excellent agreement. Second, we solve the constant μ, cylindrical wave incidence problem by an approximate but extremely useful analysis, with its validity parameters clearly established. The results, shown to bear a simple relationship to those for the one-dimension problem, enable one to make use of the one-dimension results and predict easily the penetrated fields caused by a cylindrical incident current. Then for the nonlinear μ case, we justify and extend that relationship by which the behaviors of the cylindrically diffused fields are obtained from those numerical results of the one-dimensional problem.

TABLE OF CONTENTS

LIST OF FIGURES

LIST OF FIGURES

SECTION 1. INTRODUCTION AND SUMMARY

1.1 INTRODUCTION

In protection against an EMP [1] (electromagnetic pulse), ferromagnetic metallic shielding is one of the simplest and most commonly used effective schemes [2]. The effectiveness of the shileding, measured by the ratio of the field penetrated across the shield to the incident field, depends of course on the EM properties and the geometry of the shielding material. Generally speaking, the dominant material properties are its conductivity σ and permeability μ, and, if the shielding enclosure has its radius of curvature much larger than the wave length of the incident field and is free of seams and cracks, the only important geometrical factor is the thickness of the shielding plate.

In this report, we investigated the shielding problem for the incident EMP in the form of a cylindrical TEM wave, such as a wire carrying a surge arrestor current terminated at an iron or steel shielding plane [3]. Because of the large strength of the incident field, the nonlinear ferromagnetic saturation of the plate plays an important role in determining the peak and the shape of the transmitted field. This problem, based on and together with its one-dimensional plane-wave-incidence version, is solved analytically for a constant μ case. The analytical results are then used to partly predict and to interpret the numerical results for the one-dimension nonlinear case, obtained by using a finite difference code DIFUSN, and to help predict the behaviors for the cylindrical nonlinear case.

In the following, Section 1.2 briefly summarizes the results found in this report; Section 2 solves, analytically and numerically, the one-dimension plane-wave problem; based on this, Section 3 solves the cylindrical incidence problem.

As to the system of units in this report, rationalized MKS is used.

1.2 SUMMARY

We briefly summarize here the results obtained in this report. Details of them are given in the subsequent text.

1. For wavelengths large compared to the shielding's radius of curvature, high-μ conducting plates shield EMP very effectively. For short pulse and thick slab, the diffused-through transmitted field varies as $\propto(\omega_o \mu_r \sigma^2 d^3)^{-1}$. This gives a peak transmitted field $\sim 3 \times 10^{-13}$ that of the incident peak value for a typical $\omega_o = 3 \times 10^6$ radian/sec, $\mu_r \sim 10^4$, $\sigma \sim 10^7$ mho/meter, $d \sim 3$mm. The time width of the transmitted field varies as $\propto \mu\sigma d^2$, giving $\sim 3.3 \times 10^{-1}$ sec for the typical example. This makes the shielding better for the higher frequencies, and thus substantially shifts downward the transmitted wave's frequency contents.

2. The non-linear saturation of the ferromagnetic permeability, which saturates dB/dH to smaller values for stronger field, slightly reduces the transmitted field but leaves virtually intact its time shape. This is caused by the fact that for the relatively narrow EMP in a relatively thick slab, the saturation disperses and distributes more evenly the diffused field and mitigates the build up of its local peak value, in surprising contrast to the simple intuition, naively extrapolated from the constant-μ case, that a smaller permeability admits more field in a shorter time, an extrapolation valid only when a wide pulse saturates the whole thin slab.

3. The cylindrical problem, with a wire carrying a large current, such as a surge current arrestor, terminated at a shielding wall, is solved approximately. Its results are simply related to those of the one-dimensional problem, enabling us to make

use of the one-dimensional results for the cylindrical predictions. Roughly speaking, the main part of the cylindrical diffused fields are a/ρ times that of the one-dimensional ones for $\rho \gtrsim a$ and go to zero for $\rho \to o$, with minor deviations being complicated functions of the various parameters of the problem.

The above results are found either analytically or numerically, or both. From these, we can safely conclude that for practical EMP shieldings using the highly effective high-μ conducting plates, the ferromagnetic saturation only slightly enhances the shielding effectiveness. A side result is that the presences of holes, cracks, or seams at the shielding plate probably constitute more important modes of penetration for the incident EMP.

SECTION 2. THE ONE-DIMENSION SLAB PROBLEM

2.1 ANALYSIS FOR THE CONSTANT μ CASE

Consider the one-dimensional problem depicted by Figure 1. A plane electromagnetic wave with fields

$$H^{inc}(t,z) \equiv H_y^{inc}(t,z) = H_o f(t - \frac{z}{c}) \tag{1a}$$

$$E^{inc}(t,z) \equiv E_x^{inc}(t,z) = H_o \sqrt{\frac{M_o}{\varepsilon_o}}\, f(t - \frac{z}{c}) \tag{1b}$$

is incident from $z = -\infty$ normally upon a slab of thickness d at position $z = 0$. The medium to the left and to the right of the slab is uniform and has a dielectric constant ε_o, a permeability μ_o, and a velocity of light $c \equiv (\mu_o \varepsilon_o)^{-1/2}$ [4]. The slab itself is also uniform and has a dielectric constant $\varepsilon = \varepsilon_r \varepsilon_o$, a permeability $\mu = \mu_r \mu_o$, and a conductivity σ such that

$$\sigma >> \omega\varepsilon,\ \omega\varepsilon_o \tag{2}$$

or equivalently

$$\sigma >> \left|\varepsilon \frac{\partial}{\partial t}\right|,\ \left|\varepsilon_o \frac{\partial}{\partial t}\right| \tag{2'}$$

where ω is the angular frequency of the frequency of interest. Notice that this condition of high slab conductivity is assumed <u>throughout</u> this report. In typical cases, we have $\sigma \sim 10^7$ mho/m for steel, $\varepsilon \sim 10^{-11}$ Farad/m, and $\omega \lesssim 10^7$ radian/sec for the incident EMP; thus (2) or (2') is amply satisfied. The problem is to find the electromagnetic fields everywhere, especially in and transmitted through the slab.

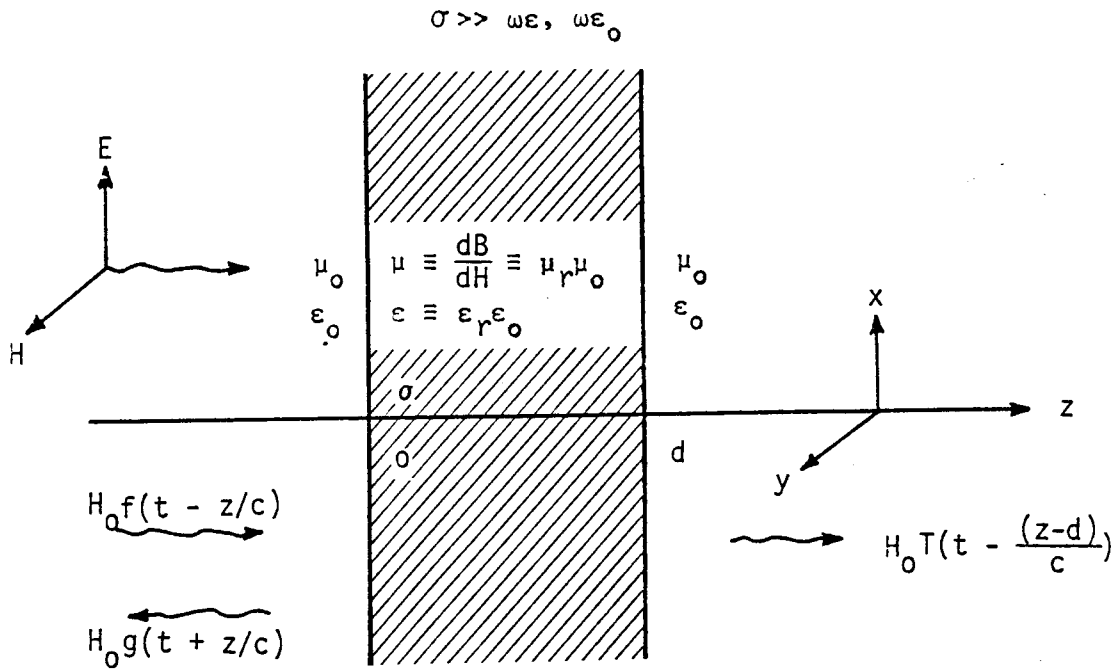

$$\begin{cases} c \equiv \dfrac{1}{\sqrt{\mu_o \varepsilon_o}} \\ f(t < 0) \equiv 0 \end{cases}$$

Figure 1. The One-Dimensional Problem

2.1.1 General Solution

Being a one-dimension problem, the only fields are plane waves with a magnetic field in the y-direction and an electric field in the x-direction. In the region $z < 0$, the reflected fields, in addition to the incident ones given by (1), are

$$H^{ref}(t,z) = H_o\, g(t + \frac{z}{c}) \tag{3a}$$

$$E^{ref}(t,z) = -H_o\sqrt{\frac{\mu_o}{\varepsilon_o}}\, g(t + \frac{z}{c}) \tag{3b}$$

In $z > 0$, the transmitted fields are

$$H^{trans}(t,z) = H_o\, T(t - \frac{(z-d)}{c}) \tag{4a}$$

$$E^{trans}(t,z) = H_o\sqrt{\frac{\mu_o}{\varepsilon_o}}\, T(t - \frac{(z-d)}{c}) \tag{4b}$$

finally, in the slab $0 < z < d$ the high conductivity condition (2) combines with the Maxwell Equations to give a simple diffusion equation

$$\frac{\partial^2}{\partial z^2} H(t,z) - \mu_r\mu_o\, \sigma\, \frac{\partial}{\partial t} H(t,z) = 0, \quad 0 < z < d \tag{5}$$

for the magnetic field $H(t,z)$ to which the electric field is related by

$$E(t,z) = \frac{-1}{\sigma}\frac{\partial}{\partial z} H(t,z) \tag{6}$$

Now to find the fields, we merely have to solve (5) and (6), subject to the boundary conditions that require continuous magnetic and electric fields at both slab surfaces $z = 0$ and $z = d$. In terms of the magnetic field in the slab, these conditions are (Appendix A)

$$\frac{\partial}{\partial z} H(t,0) - \sqrt{\frac{\mu_o}{\varepsilon_o}}\,\sigma H(t,0) = -2\sqrt{\frac{\mu_o}{\varepsilon_o}}\,H_o\sigma\, f(t) \tag{7a}$$

$$\frac{\partial}{\partial z} H(t,d) + \sqrt{\frac{\mu_o}{\varepsilon_o}}\,\sigma H(t,d) = 0 \tag{7b}$$

Thus, the problem reduces to solving (5) and (7).

To express the field in a convenient and simple form, we make use of the Laplace transform

$$\hat{H}(s,z) = \int_o^\infty H(t,z)\, e^{-st}\, dt \equiv L[H(t,z)] \tag{8}$$

Then from (5) and (7), the resulting transformed fields in $0 \leq z \leq d$ are (Appendix B)

$$\hat{H}(s,z) = 2H_o\, \hat{f}(s) \left[A(s)\, e^{-\sqrt{\mu\sigma s}\, z} + B(s)\, e^{\sqrt{\mu\sigma s}\, z}\right] \tag{9a}$$

$$\hat{E}(s,z) = -2H_o\, f(s)\sqrt{\frac{\mu s}{\sigma}} \left[-A(s)\, e^{-\sqrt{\mu\sigma s}\, z} + B(s)\, e^{\sqrt{\mu\sigma s}\, z}\right] \tag{9b}$$

where

$$\begin{pmatrix} A(s) \\ B(s) \end{pmatrix} = \frac{\begin{pmatrix} 1 + \sqrt{\frac{\mu_r \varepsilon_o s}{\sigma}} \\ -\left(1 - \sqrt{\frac{\mu_r \varepsilon_o s}{\sigma}}\right) e^{-2\sqrt{\mu\sigma s}\, d} \end{pmatrix}}{\left(1 + \sqrt{\frac{\mu_r \varepsilon_o s}{\sigma}}\right)^2 - \left(1 - \sqrt{\frac{\mu_r \varepsilon_o s}{\sigma}}\right)^2 e^{-2\sqrt{\mu\sigma s}\, d}} \tag{9c}$$

In particular, this gives the transmitted magnetic field

$$H_o\hat{T}(s) = \hat{H}(s,d) = \frac{4\sqrt{\frac{\mu_r\varepsilon_o s}{\sigma}}\, H_o\, \hat{f}(s)\, e^{-\sqrt{\mu\sigma s}\, d}}{\left(1+\sqrt{\frac{\mu_r\varepsilon_o s}{\sigma}}\right)^2 - \left(1-\sqrt{\frac{\mu_r\varepsilon_o s}{\sigma}}\right)^2 e^{-2\sqrt{\mu\sigma s}\, d}} \qquad (10)$$

$$= \frac{2\, H_o\, \hat{f}(s)\sqrt{\frac{\mu_r\varepsilon_o s}{\sigma}}}{Sh\left(\sqrt{\mu\sigma s}\, d\right)}\,, \quad \text{if } \sqrt{\frac{\mu_r\varepsilon_o s}{\sigma}} << 1 \qquad (10')$$

and the total magnetic field at the incidence side of the slab

$$H_o[\hat{f}(s)+\hat{g}(s)] = \hat{H}(s,0) = \frac{2H_o\, \hat{f}(s)\left[\left(1+\sqrt{\frac{\mu_r\varepsilon_o s}{\sigma}}\right) - \left(1-\sqrt{\frac{\mu_r\varepsilon_o s}{\sigma}}\right) e^{-2\sqrt{\mu\sigma s}\, d}\right]}{\left(1+\sqrt{\frac{\mu_r\varepsilon_o s}{\sigma}}\right)^2 - \left(1-\sqrt{\frac{\mu_r\varepsilon_o s}{\sigma}}\right)^2 e^{-2\sqrt{\mu\sigma s}\, d}}$$

(11)

$$= 2H_o\, \hat{f}(s)\left[1 - \frac{1+0\left(\frac{\mu_r\varepsilon_o s}{\sigma}\right)}{2+\sigma d\sqrt{\frac{\mu_o}{\varepsilon_o}}}\right]$$

$$\text{if } s \to 0,\ \sqrt{\frac{\mu_r\varepsilon_o s}{\sigma}}\,,\ \sqrt{\mu\sigma s}\, d << 1 \qquad (11')$$

$$= 2H_o\, \hat{f}(s)\left[1 - \sqrt{\frac{\mu_r\varepsilon_o s}{\sigma}}\,\frac{1+e^{-2\sqrt{\mu\sigma s}\, d}}{1-e^{-2\sqrt{\mu\sigma s}\, d}}\right]$$

$$\text{if } \sqrt{\frac{\mu_r\varepsilon_o s}{\sigma}} << 1,\ \sqrt{\mu\sigma s}\, d \not<< 1 \qquad (11'')$$

From these expressions, various approximate simple formulas can be derived for fields in the time domain, as will be shown in the following. Such formulas serve to predict the approximate physical behaviors of the fields and to give insights and provide cross checks to the numerical results. Only response to a delta-incidence, $H^{inc} = \delta(t - \frac{z}{c})$, is examined in detail analytically. Responses to other incidences can be obtained by a convolution. In particular, the response to a "narrow" incident pulse is obtained by simply multiplying the time-integrated area under that pulse by the δ-response. The condition for such a "narrowness" is

$$t \text{ lies in } \{t^{(\delta)}\} \text{ and } (t >> \Delta t_o) \tag{12}$$

where $\{t^{(\delta)}\}$ are the times in which the δ-response expression is valid and Δt_o is the time-width of the incident pulse.

2.1.2 Fields Near the Incident Surface in a Thick Slab

First, for incident waves with frequency contents not too large nor too small

$$\sqrt{s} << \sqrt{\frac{\sigma}{\mu_r \varepsilon_o}}$$

$$\sqrt{s} \not< \frac{1}{\sqrt{\mu\sigma}\, d} \tag{13}$$

or, equivalently, at times not too early nor too late

$$\sqrt{t} >> \sqrt{\frac{\mu_r \varepsilon_o}{\sigma}}$$

$$\sqrt{t} \not> \sqrt{\mu\sigma}\, d \tag{13'}$$

Equation (12) clearly gives $\hat{H}(s,0) = 2H_o \hat{f}(s)$, a total magnetic field at the incident side of a highly conductive thick slab being twice the incident value, as it should be. If the incident pulse has its peak time within (13'), as is usually the case for EMP, then at position $z = 0$ the magnetic field has its peak time the same as that of the incident one, but has its peak value twice that of the incident one.

Second, under a restriction on the frequency or time ranges that differs slightly from (13),

$$\sqrt{\frac{24\ \sigma}{\mu_r \varepsilon_o}} >> \sqrt{s} >> \frac{1}{\sqrt{\mu\sigma}\ d} \tag{14}$$

or equivalently

$$\sqrt{\frac{\mu_r \varepsilon_o}{24\ \sigma}} << \sqrt{t} << \sqrt{\mu\sigma}\ d \tag{14'}$$

and at positions in the slab near but not on the left surface and not close to the right surface such that

$$\frac{1}{2\sigma\sqrt{\frac{\mu_o}{\varepsilon_o}}} << z << \sqrt{6}\ d \tag{15}$$

the field can be obtained from (9) by ignoring terms containing $\exp(-\sqrt{\mu\sigma s}\ d)$. Such a magnetic field, for a δ-incidence, is (Appendix C)

$$H^{(\delta)}(t,z) = \sqrt{\mu\sigma}\ \frac{e^{-\mu\sigma z^2/4t}}{\sqrt{\pi t}}\ \frac{z}{t + \frac{\mu_r z}{2ct}} \tag{16}$$

As a function of time, at a <u>given z</u> satisfying (15), the magnetic field (16) has its peak value

$$H^{(\delta)}(t_{pk/z},z) = \sqrt{\frac{\sigma}{\pi e^3}} \frac{1}{t^{(\delta)}_{pk/z}\left(1 + \frac{z\mu_r}{\mu\sigma c z}\right)} \tag{17a}$$

at the peak-time (with given z as a parameter)

$$t^{(\delta)}_{pk/z} = \frac{\mu\sigma z^2}{\sigma} \tag{17b}$$

Obviously, the condition (15) on z ensures that $t^{(\delta)}_{pk/z}$ satisfies the condition (14') on t, and therefore the results (17) are valid under the sole restriction (15).

Viewed differently as a function of position, at a <u>given t</u> satisfying (14'), the magnetic field (16) has its maximum value

$$H^{(\delta)}(t,z_{max/t}) = \sqrt{\frac{2}{\pi e}} \frac{1}{t\left(1 + \sqrt{\frac{\varepsilon_o}{2\mu_r\sigma t}}\right)} \tag{18a}$$

at the maximum-position (with given t as a parameter)

$$z^{(\delta)}_{max/t} = \sqrt{\frac{2t}{\mu\sigma}} \tag{18b}$$

which diffuses to the right with velocity

$$v^{(\delta)}_{z_{max/t}}(t) \equiv \frac{d}{dt} z^{(\delta)}_{max/t} = \frac{1}{\sqrt{2\mu\sigma t}} \tag{18c}$$

Again, the condition (14') on t ensures that $z^{(\delta)}_{max/t}$ satisfies the condition (15) on z, and therefore the results (18) are valid under the sole restriction (14').

2.1.3 Fields at the Shielded Surface of the Slab

For a highly conductive slab satisfying the first inequalities in (14) and (14'), without any restriction on the slab thickness, the δ-response transmitted magnetic field at z = d is (Appendix C)

$$H^{(\delta)}(t,d) = \sqrt{\frac{\mu_r \varepsilon_o}{\pi\sigma}} \frac{1}{t^{5/2}} \sum_{n=1}^{\infty} [(2n-1)^2 \mu\sigma d^2 - 2t]\, e^{\frac{-(2n-1)^2 \mu\sigma d^2}{4t}} \tag{19}$$

At times that (19) is valid and converges fast,

$$\sqrt{\mu_r \varepsilon_o/\sigma} << \sqrt{t} \lesssim \frac{\sqrt{\mu\sigma}\, d}{2} \quad , \tag{20}$$

(19) reduces to

$$H^{(\delta)}(t,d) = \sqrt{\frac{\mu_r \varepsilon_o}{\pi\sigma}} \frac{(\mu\sigma d^2 - 2t)\, e^{\frac{-\mu\sigma d^2}{4t}}}{t^{5/2}} \tag{21}$$

This transmitted field has its peak amplitude

$$H^{(\delta)}(t_{pk/d},d) = \frac{(1-2\beta)\, e^{-1/4\beta}}{\sqrt{\pi}\, \beta^{5/2}} \frac{1}{\mu\sigma d^2\, \sigma d \sqrt{\frac{\mu_o}{\varepsilon_o}}}$$

$$= 6.25 \times 10^{-2} \times \frac{1}{\mu_r \left(\frac{\sigma}{2\times 10^7}\right)^2 \left(\frac{d}{10^{-3}}\right)^3} \tag{22a}$$

at a peak time

$$t^{(\delta)}_{pk/d} = \mu\sigma d^2\beta \equiv \mu\sigma d^2 \cdot \frac{1 - \sqrt{2/3}}{2} = 2.31 \times 10^{-6}\ \mu_r\left(\frac{\sigma}{2\times10^7}\right)\left(\frac{d}{10^{-3}}\right)^2 \tag{22b}$$

The time-width of the peak at 10^{-1} strength is

$$(\Delta t_{pk/d})_{1/10} \sim 0.3\ \mu\sigma d^2 = 7.54 \times 10^{-6}\ \mu_r\left(\frac{\sigma}{2\times10^7}\right)\left(\frac{d}{10^{-3}}\right)^2 \tag{22c}$$

Notice that the second inequality of (20) is always satisfied by $t^{(\delta)}_{pk/d}$, and the first one is also satisfied by $t^{(\delta)}_{pk/d}$ if

$$1 << \left(\sigma d \sqrt{\frac{\mu_o}{\varepsilon_o}}\right) \tag{23}$$

For real shielding problems, (23) is always amply satisfied. Thus, results (21) and (22) are valid approximations in the realistic time interval of interest (20).

Before going into the nonlinear case, we make the side remark that the transmitted field $\hat{H}(s,d)$ for a slab of thickness d is much smaller than the transmitted field $\hat{H}^{(\infty)}(s,d)$ at a depth d in a semi-infinite (half-space) slab of the same material. In fact, for $\sigma >> \mu_r\varepsilon_o s$, their ratio is

$$\frac{H(s,d)}{H^{(\infty)}(s,d)} \sim \frac{2\sqrt{\frac{\mu_r\varepsilon_o s}{\sigma}}}{1 + e^{-2\sqrt{\mu\sigma s}\ d}} << 1 \tag{24}$$

Intuitively, this is clearly plausible because the diffused field reaching z = d will leave the slab surface and propagate into z > d much faster for the d-thick slab case than it does for the semi-infinite slab case, and therefore the H(s,d) has less opportunity to pile up than the $H^{(\infty)}(s,d)$ does.

2.2 THE NONLINEAR μ CASE

For a ferromagnetic material, the permeability depends on the magnetic field strength, and it is the differential permeability

$$\frac{dB}{dH} = \mu(H) \equiv \mu_R(H)\ \mu_o \tag{25}$$

that enters the field equation [5]. In a strict sense, hysteresis makes dB/dH not a single valued function of H. However, for the transient field behaviors, not the steady state behavior, that we are investigating, we can use approximately [6] the magnetization curve B(H) to get $\mu_R(H)$. Such a $\mu_R(H)$ for a typical iron saturates at a magnetic field strength H_c of the order of several hundreds of amp/m, from a $\mu_R(H<H_c) \sim 10^4$ to 10^3 to a $\mu_R(H>H_c) \sim 10$ to 1, in a range of change in H of the order of tens of amp/meter.

A very simple expression to approximately fit such a magnetization curve can be

$$\mu_R(H) = 1 + \frac{\mu_{Ro} - 1}{1 + e^{\alpha(H-H_c)}} \tag{26}$$

where $\mu_{Ro} >> 1$ and $e^{\alpha H_c} >> 1$. This fit gives a $\mu_R(0) \sim \mu_{Ro}$, a $\mu_R(H>>H_c) \sim 1$, and makes the saturation transition occur in a range $\Delta H \sim 1/\alpha$ about $H \sim H_c$. The no-saturation case is simply represented by $H_c \to \infty$.

In the following, we first make several theoretical remarks, then solve the nonlinear μ problem numerically, and finally establish the agreement between the numerical and the analytical results.

2.2.1 Theoretical Remarks

For the linear μ case, μ being a constant throughout the whole slab and independent of time, at fixed positions in the slab a smaller μ results in a stronger diffused field ($\propto \mu^{-1}$, see (17a) and (22a)) being diffused to there in a shorter time ($\propto \mu$, see (17b) and (22b)). Viewed differently at fixed times, the spatial profile of the field diffuses and reaches its "equilibrium" shape, peaked and symmetric about the center of the slab after the incident pulse, faster (diffusion distance and velocity $\propto \mu^{-1/2}$, see (18)). As a result, a constant smaller μ not only enhances the diffused and transmitted fields, but also enhances the higher-frequency part more than it does the lower frequency part. The latter statement can be seen for the case of interest $(\mu_r \varepsilon_o s/\sigma)^{1/2} << 1$ from (Appendix D)

$$\left(\frac{\hat{H}(s_>,d)}{\hat{H}(s_<,d)}\right)_{\mu_<} \Bigg/ \left(\frac{\hat{H}(s_>,d)}{\hat{H}(s_<,d)}\right)_{\mu_>} = \frac{Sh(d\sqrt{\sigma\mu_< s_<})}{Sh(d\sqrt{\sigma\mu_< s_>})} \frac{Sh(d\sqrt{\sigma\mu_> s_>})}{Sh(d\sqrt{\sigma\mu_> s_<})} > 1 \qquad (27)$$

where $\mu_> > \mu_<$ and $s_> > s_<$, or from (16), (17), (21), (22) directly.

Now for a slab with a nonlinear μ, which saturates to smaller values where the field is stronger, the diffusion results are very different but can still be carefully extrapolated from the linear results. First, at constant times the spatial profile has its strong-field center part diffuse faster than the low-field edge part. Thus the strong-field spreads out in a wider range and retains a lower value than it does without saturation, and it overtakes but is "confined" by the low-field edge part, in a manner somewhat similar to a shock phenomenon. In short, the saturation makes strong fields diffuse more easily, and thus acts to distribute the field more evenly and mitigates the build-up of a localized strong field.

Second, if the pulse time-width is long compared with the saturated peak-diffusion-time through the slab, $t_{pk/d}$ with $\mu = \mu_{saturated}$ (see (22b)), then the diffused and transmitted fields behave the same as if the whole slab has the smaller permeability $\mu_{saturated}$--with larger peaks and shorter times as described above in the beginning paragraph. However, if the pulse width is short, i.e.,

$$\Delta t_o < t_{pk/d,\mu_{saturated}} \leftrightarrow \Delta t_o < \frac{1 - \sqrt{2/3}}{2} \cdot \mu_{saturated}\, \sigma d^2 \tag{28}$$

and the slab is thick relative to the incident wave such that the transmitted magnetic field is much smaller than the H_c, i.e.,

$$6.25 \times 10^{-2} \times \frac{H_o\, \Delta t_o}{\mu_r \left(\frac{\sigma}{2\times10^7}\right)^2 \left(\frac{d}{10^{-3}}\right)^3} << H_c \tag{29}$$

the maximum field at given times and the peak transmitted field at $z = d$ becomes <u>smaller</u> than they are without saturation, due to the first effect just mentioned. For a highly conductive slab that has $\sigma >> \omega_o \varepsilon_o \mu_R(H)$, saturated or not, the amount of field admitted into the slab, from (11"), is virtually independent of μ. The maximum field at a given time is roughly inversely proportional to its spatial spread at that time. Thus, approximately we have the ratio of the maximum transmitted fields with saturation to that without saturation (Appendix E)

$$\frac{H(t_{pk/d},d)^{(\text{N.L. sat.})}}{H(t_{pk/d},d)^{(\text{no sat.})}} \sim \frac{z_{max/t_c}^{(\text{no sat.})}}{z_{max/t_c}^{(\text{N.L. sat.})}} \tag{30}$$

where the superscripts N.L. sat. and no sat. denote, respectively, the case of nonlinear saturation and no saturation, the t_c is the time at

As outputs it gives at each time step the fields at some selected fixed positions, including of course z = 0 and z = d, the value and the location of the maximum magnetic field (in $0 \leq z \leq d$) at that time, and the two locations between which the magnetic field at that time exceeds a selected value such as the H_c about which the saturation occurs. A listing of the code DIFUSN is included in Appendix F.

Numerical results for a number of parameter values of practical interest are obtained and plotted. In these results, the $\mu_R(H)$ of (26) is taken to represent the non-linear permeability, and the expression

$$H^{inc}(t,z) = H_o \sin^2 \omega_o(t-\frac{z}{c}), \quad 0 \leq t-\frac{z}{c} \leq \frac{\pi}{\omega_o}$$

$$= 0, \quad \text{otherwise} \tag{32}$$

is used as the incident wave. The resulting plots and their comparisons with analysis are given in the following.

The results for a typical example of iron shielding with a $\mu_R(H)$ whose $\mu_{Ro} = 10^4$, $H_c = 400$ amp/m, and $\alpha = 1/50$ m/amp, a thickness d = 3 mm, a conductivity $\sigma = 10^7$ mho/m, and an incident $H_o = 10^5$ amp/m and $\omega_o = 3 \times 10^6$ rad/sec are plotted in Figure 2 to Figure 5. Corresponding results for this same case but with constant $\mu_r = \mu_{Ro} = \mu_R(0)$ and $\mu_r = 1 = \mu_R(\infty)$, the limiting values of the nonlinear $\mu_R(H)$, are also computed and plotted together. The plots show the maximum magnetic field $H(t,z_{max/t})$ of the diffusion profile first increases as twice the incident wave (Figure 2-1) at the incident surface of the slab (Figure 2-2), then breaks away from the incident wave and decreases (Figures 2-1, 3-1, 4-1) while diffusing into and toward the center of the slab (Figures 2-2, 3-2, 4-2). For the constant μ cases, the values and the location of $H(t,z_{max/t})$ agree very well with those given in (18) (in its region of validity (14') of course) from the previous analysis (labeled curved in Figures 2-1, 3-1, 3-2, 4-1, 4-2).

which the maximum magnetic field for the no-saturation case decreases through the H_c, and z_{max/t_c} is the distance the maximum field reaches at time t_c. From (2-18) and of course under its validity condition (14'), we can express

$$z_{max/t_c}^{(no\ sat.)} \sim \left(\frac{2\sqrt{2/\pi e} \cdot H_o \Delta t_o}{\mu_{Ro} \mu_o \sigma H_c} \right)^{1/2} \tag{31}$$

The value of $z_{max/t_c}^{(N.L.\ sat.)}$, larger than $z_{max/t}^{(no\ sat.)}$ as discussed in the first remark, cannot be obtained analytically in the present analysis, but its numerical value can be used, together with (31), in (30) to relate the nonlinear maximum transmitted field to the linear one.

Third, the $t_{pk/d}$ and the $(\Delta t_{pk/d})_{1/10}$ for the nonlinear case is about the same as that of the no-saturation case, as long as (28) and (29) are satisfied. For under such conditions the field is well dispersed below H_c long before it diffuses to z = d, and thus it is the unsaturated μ_{Ro} that controls the $t_{pk/d}$.

Finally, for the EMP shielding cases of practical interest, (28) and (29) are satisfied. This is easily seen by substituting typical numbers into those expressions. Thus, the above observations are practically applicable.

2.2.2 Numerical Method and Results

The numerical code DIFUSN solves the one-dimensional nonlinear μ diffusion problem by finitely differencing (5) and (7) with $\mu_R(H)$ replacing the constant μ_R. An implicit "T" finite difference scheme, stable in the round-off error and the differencing grid sizes, is used [7]. The code takes as inputs any nonlinear function $\mu_R(H)$, any incident pulse shape $H_o f(t)$, and the properties μ_o, ε_o of the ambient medium and ε, σ, d of the slab.

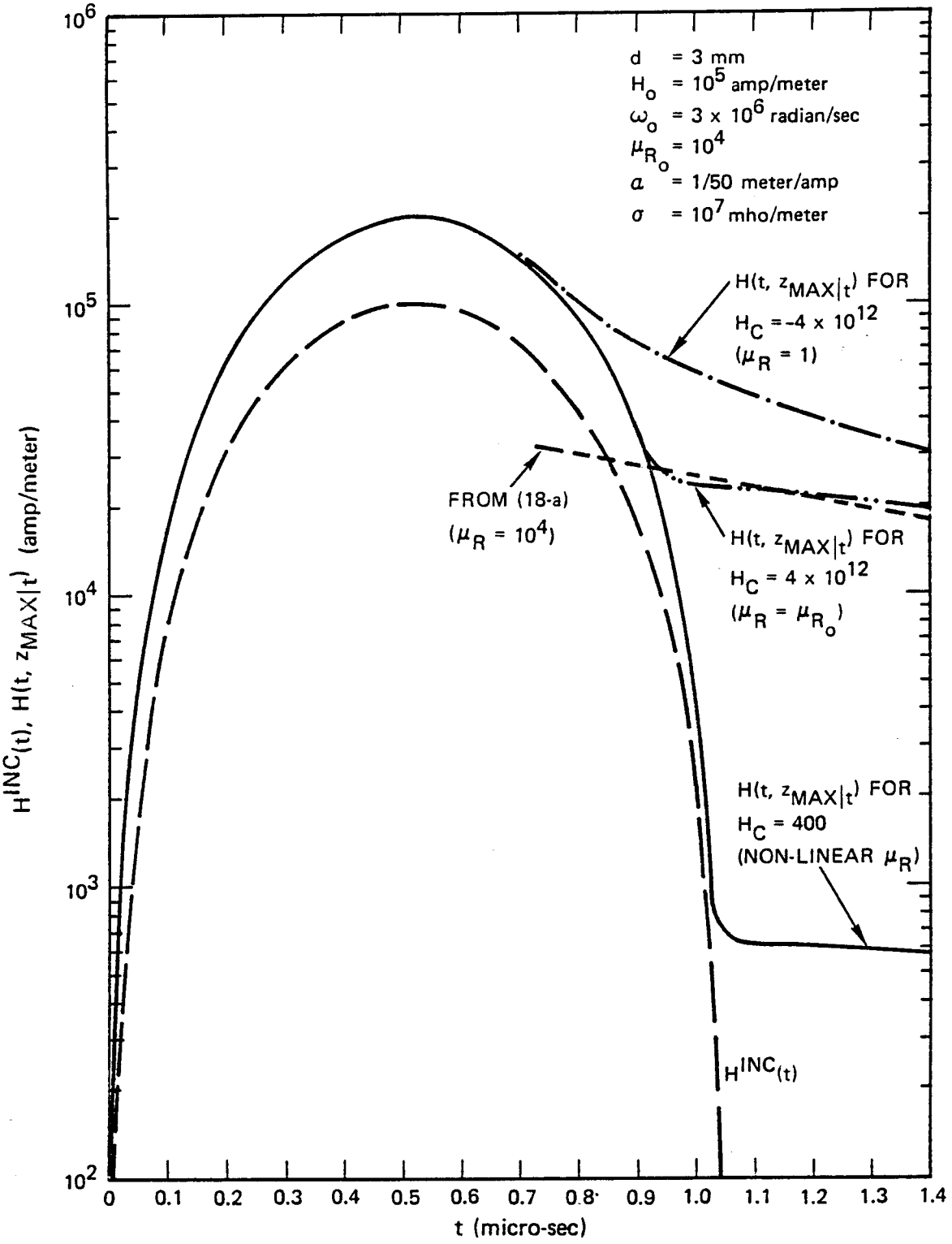

Figure 2-1. The Incident Magnetic Field and the Maximum Magnetic Field $H(t, z_{max|t})$ as Functions of Time

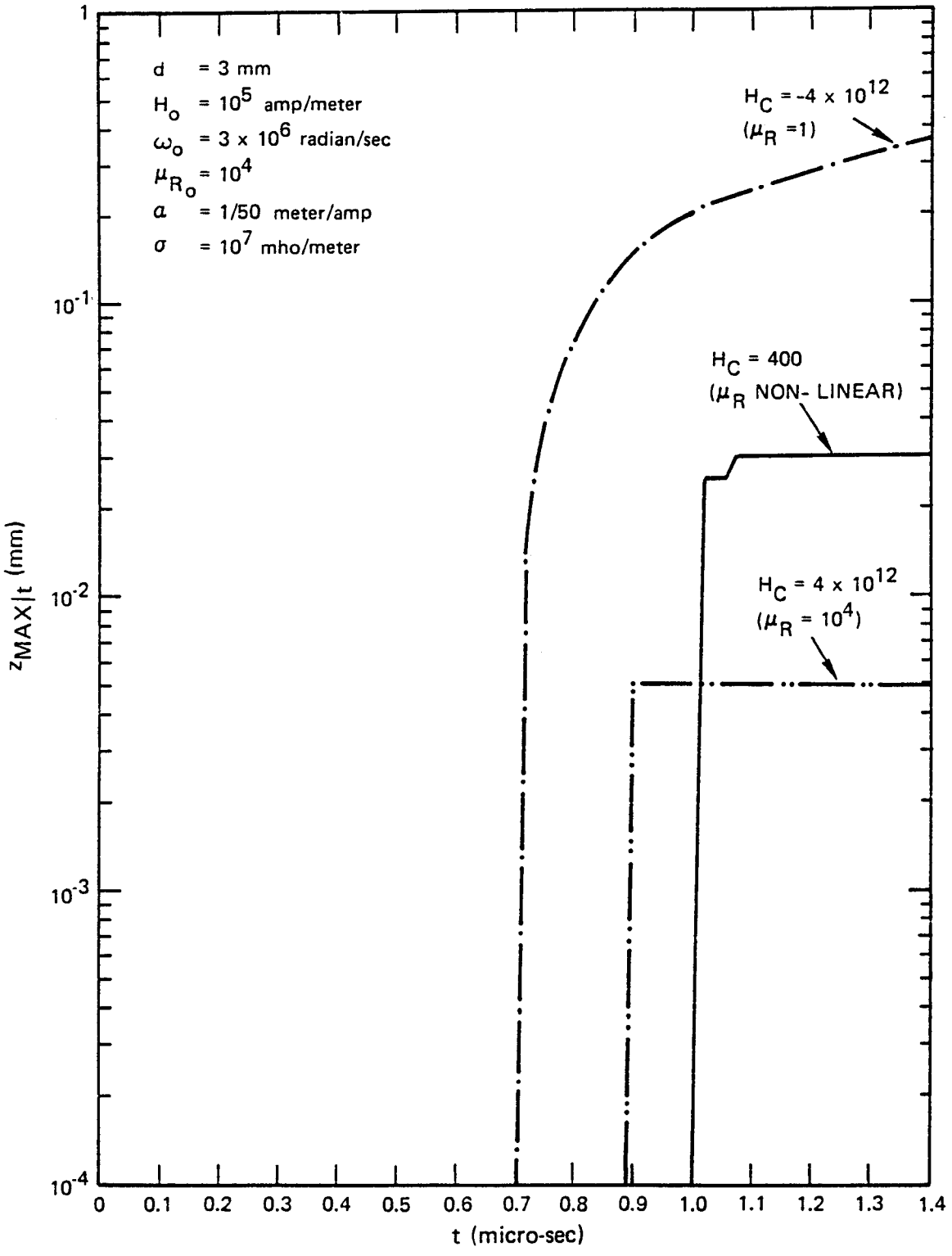

Figure 2-2. The $z_{max|t}$ for the Maximum Field as Functions of Time

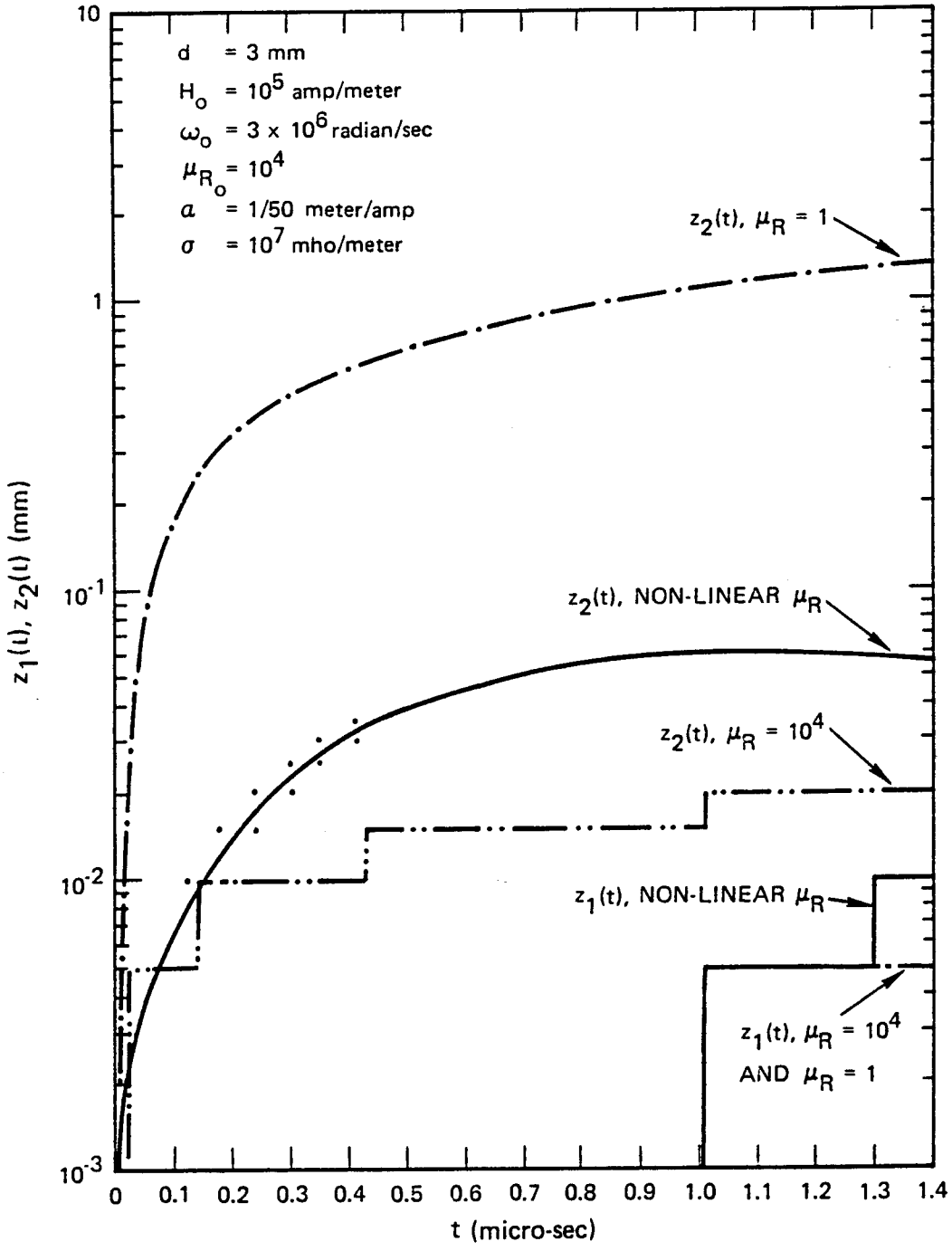

Figure 2-3. The Boundary of the Region $z_1(t) < z < z_2(t)$ in which H(t, z) Exceeds 400, The H_c for the Non-Linear μ_R

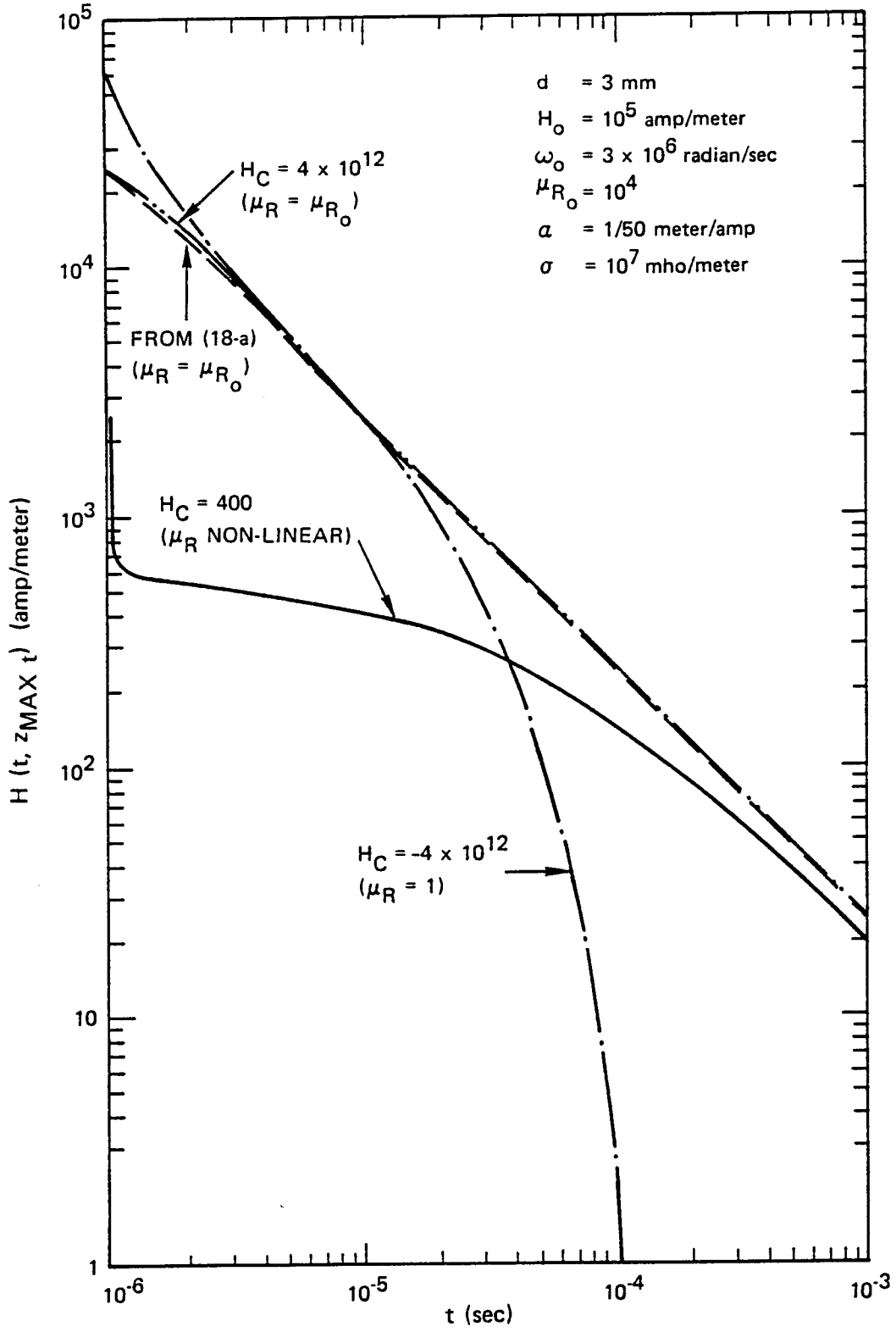

Figure 3-1. The Maximum Fields in the Slab H(t, $z_{max|t}$) as Functions of Time (Continuation of Fig. 2-1)

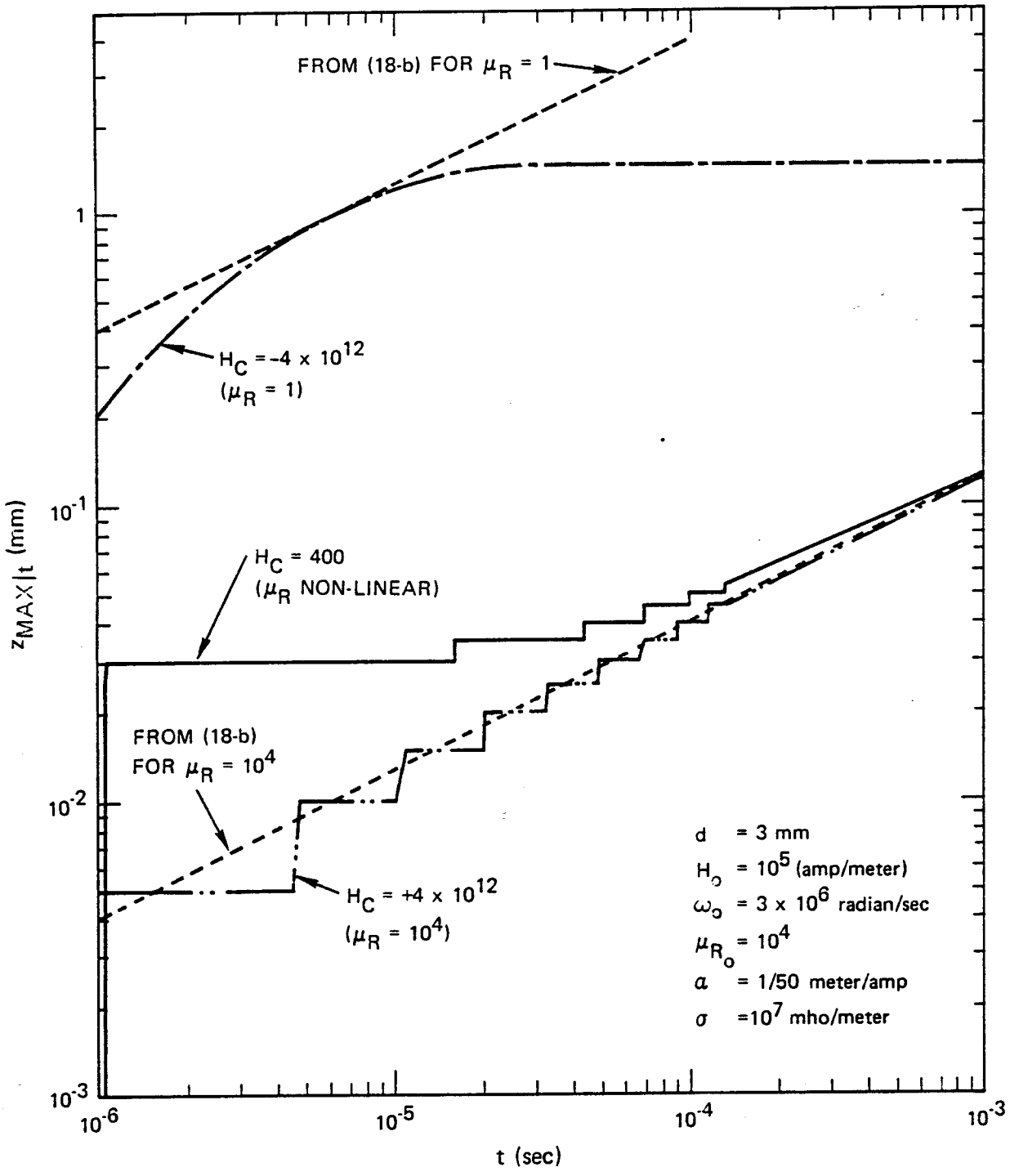

Figure 3-2. The $z_{max|t}$ for the Maximum Magnetic Field in the Slab as Functions of Time (Continuation of Fig. 2-2)

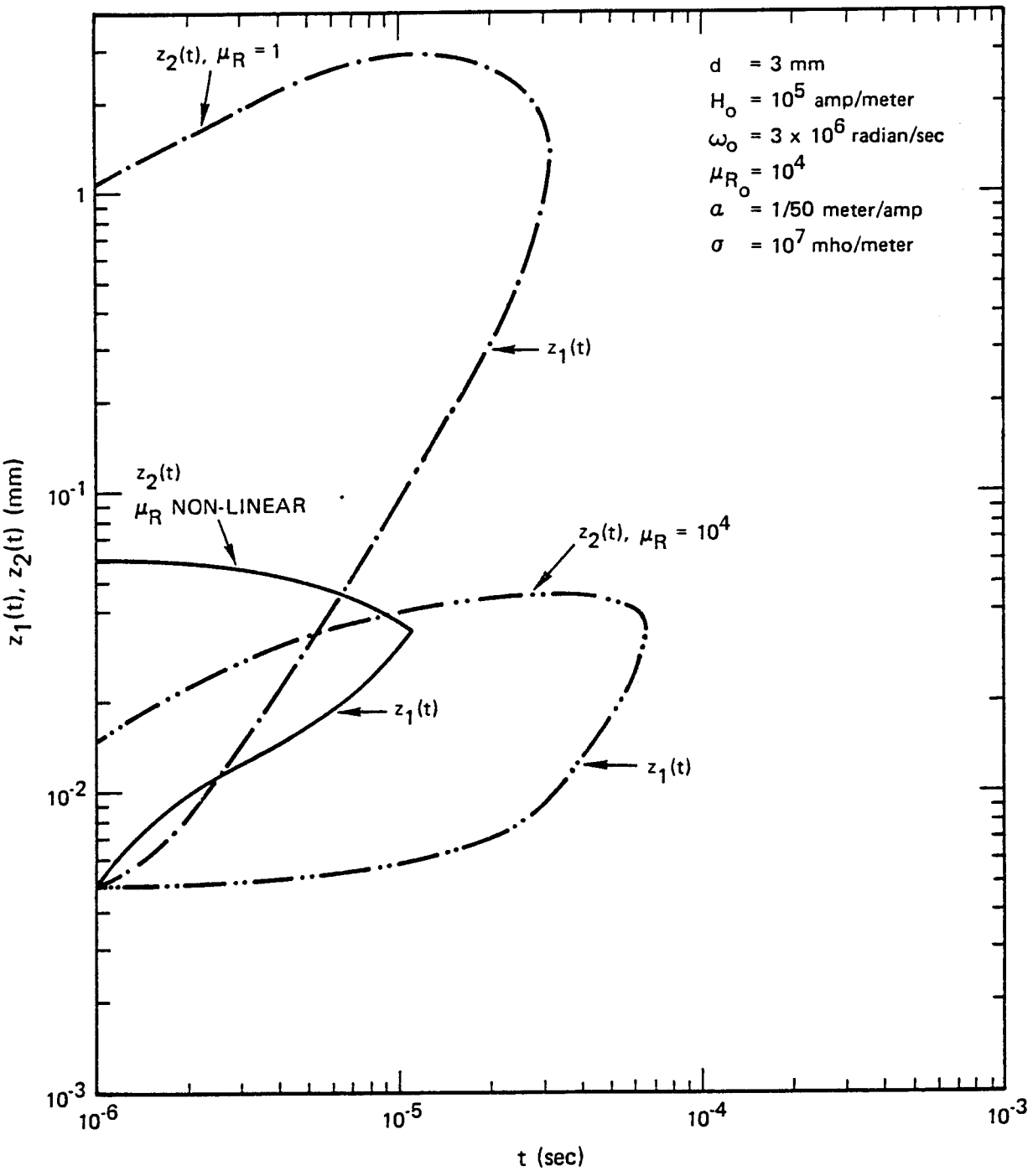

Figure 3-3. The Boundary of the Region $z_1(t) < z < z_2(t)$ in which $H(t,z)$ Exceeds 400, the H_c for the Non-Linear μ_R Case
(Continuation of Fig. 2-3)

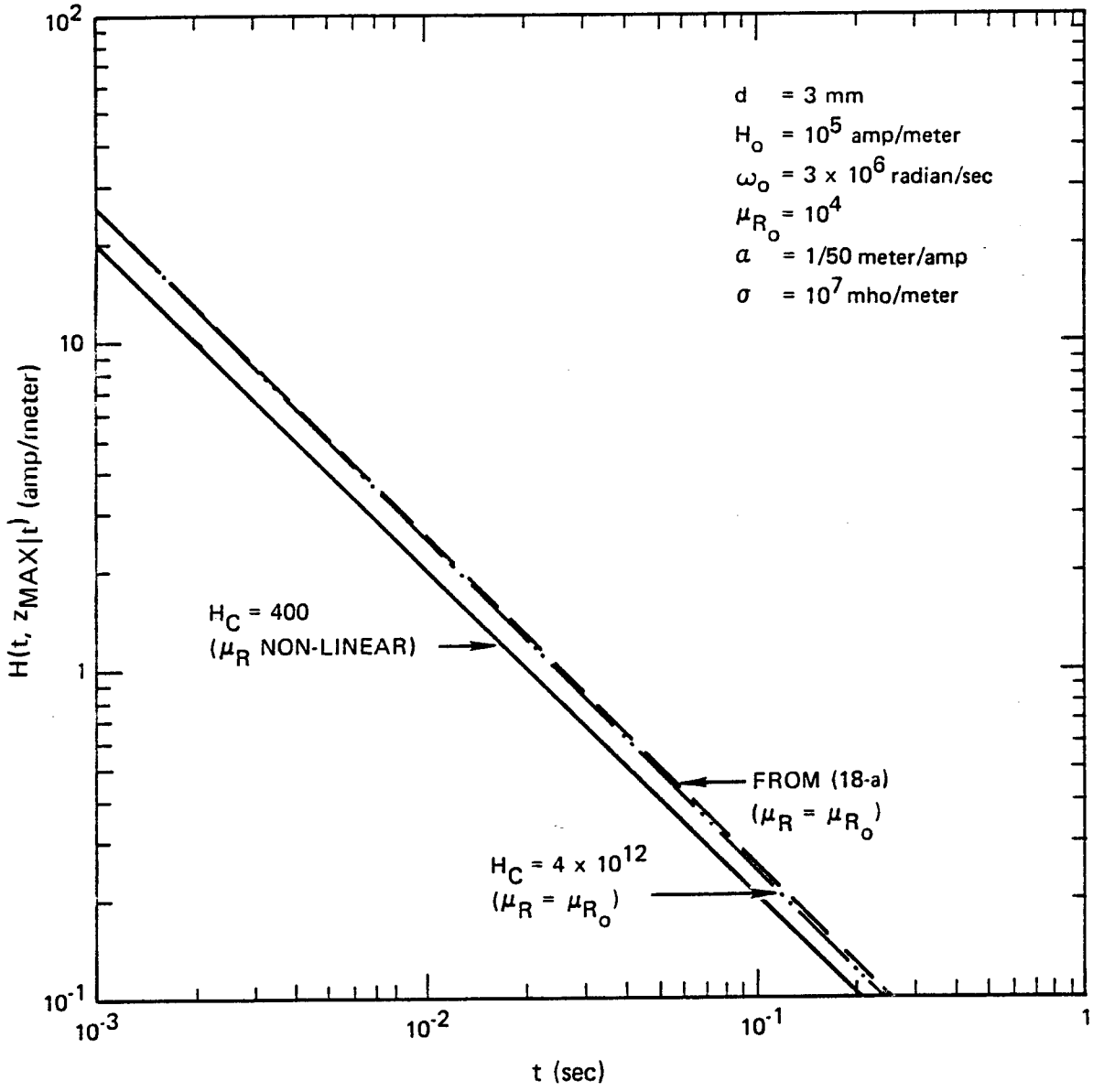

Figure 4-1. Continuation of Fig. 3-1

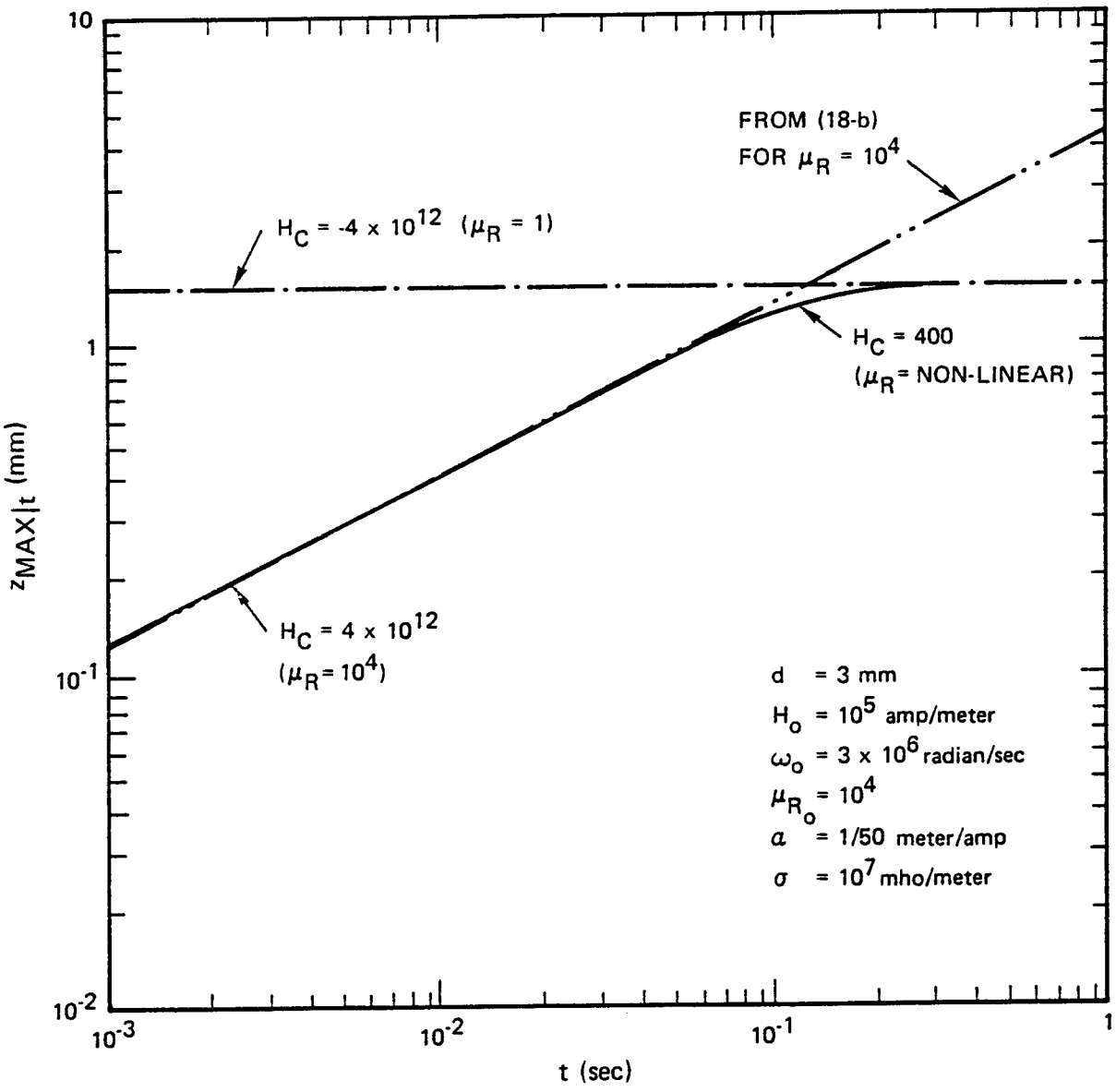

Figure 4-2. Continuation of Fig. 3-2

The value of $H(r,z_{max/t})$ for the nonlinear μ case must be less than the larger of those for the corresponding limiting constant μ cases; it approaches that for $\mu_r = 1$ if the pulse has long duration and strong amplitude to saturate the whole thin slab (i.e., (28) and (29) inequalities reversed), and vice versa. But it does not do so monotonically, because of the competing saturation effect, causing the strong field near the $z = 0$ end to diffuse faster both in the $+z$ direction penetrating the slab and in the $-z$ direction escaping the slab. The location $z_{max/t}$ of $H(t,z_{max/t})$ for the nonlinear μ case, however, always lies between those for the corresponding constant μ cases (Figures 2-2, 3-2, 4-2), as it should, because the smaller saturated μ under the peak permits it to diffuse faster. Further, the spatial region within which the $H(t,z)$ exceeds the H_c of the nonlinear μ case is plotted (Figures 2-3, 3-3). This region is roughly the extent within which the nonlinear saturation occurs, and its disappearance marks approximately the end of the saturation effect.

The transmitted magnetic fields $H(t,d)$ for various parameters are shown in Figure 5 to Figure 9. First, the limiting constant μ results exhibit excellent agreement with the analytical formulas (21) and (22), for the typical example (Figure 5) and for other variations of parameters (not plotted), when the (practical) thick plate condition (23), thus the condition (20), and the short pulse condition (28) are satisfied. Second, satisfying the additional but still practical condition (29), the $H(t,d)$ in the typical nonlinear example has the same time shape as but is slightly lowered near its peak by a factor ~ 0.8 from the $H(t,d)$ in the same typical example but with a constant $\mu_r = \mu_{Ro}$ (Figure 5). This agrees with (30) as it should. Third, under the restrictive but practical conditions (23), (28) and (29), the $H(t,d)/H_o$ with different H_o substituted in the typical nonlinear problem (Figure 6) decreases slightly near its peak for larger H_o, approximately according to (30), but has its time shape virtually unchanged. This is as expected from Section 2.2.1. Similar variations in ω_o, in view of the multiplicative factor $\pi H_o/(2\omega_o)$ to convert the δ-response to the narrow-pulse-response (32), expectedly

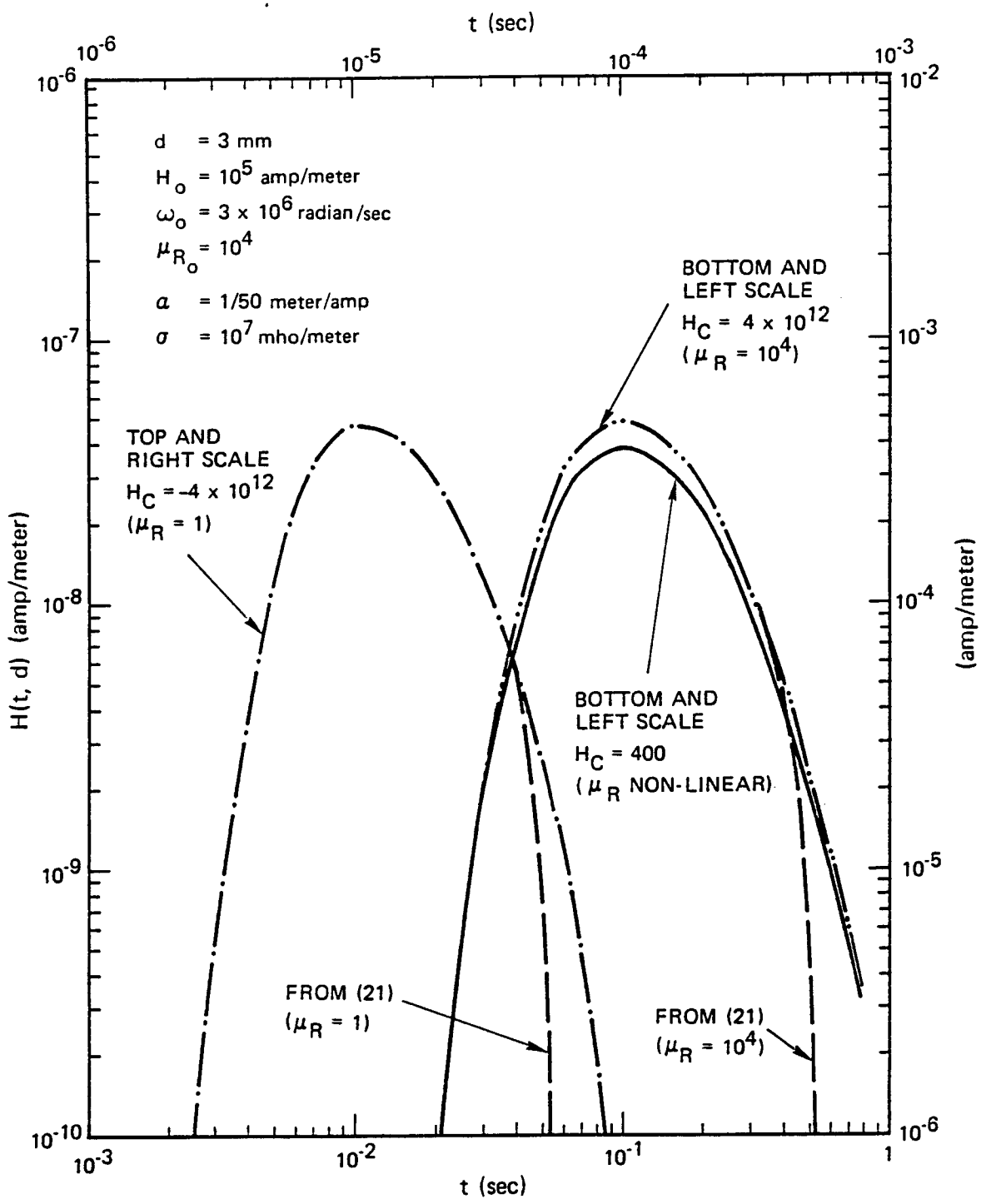

Figure 5. The Transmitted Magnetic Fields H(t, d) as Functions of Time

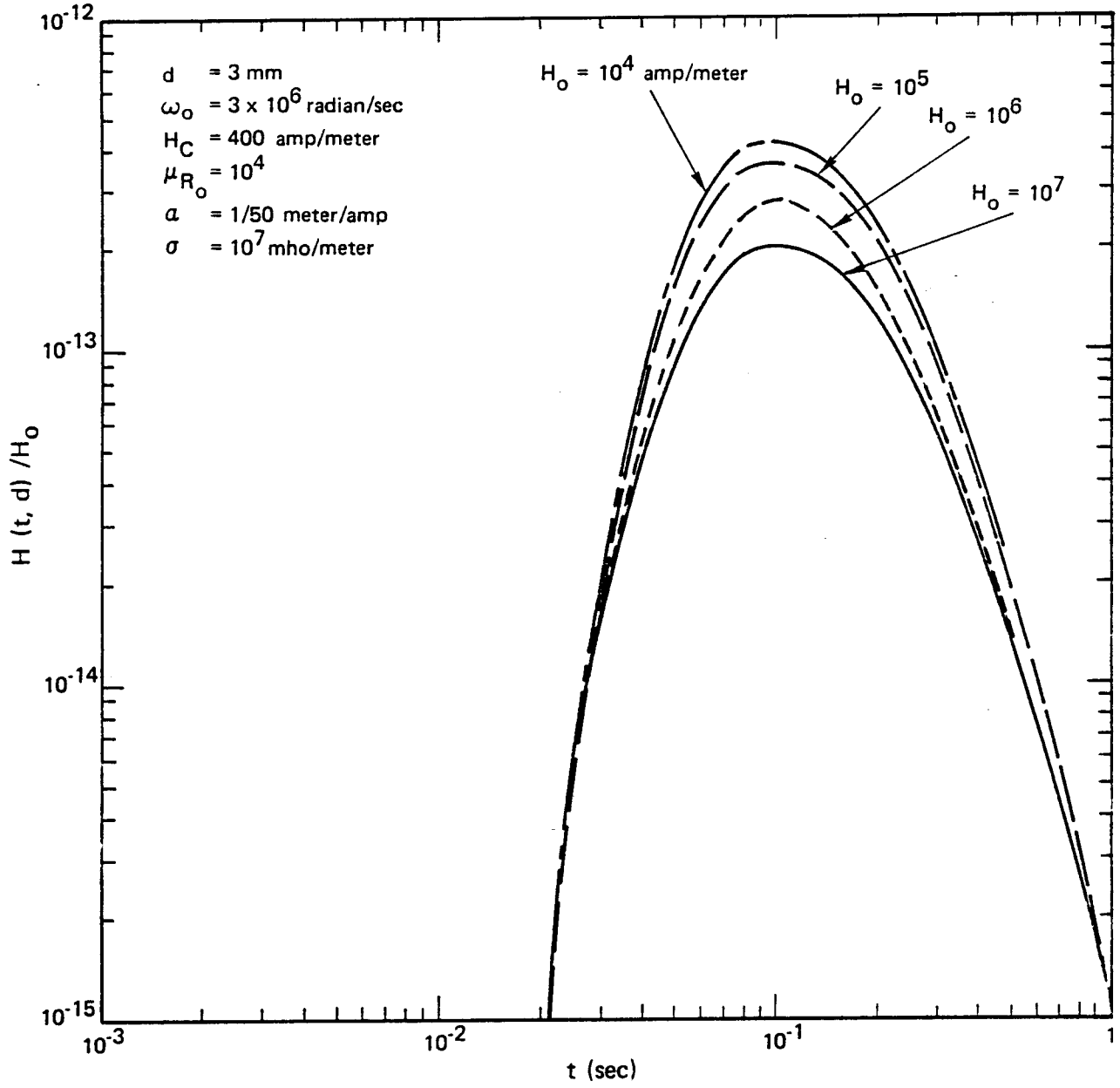

Figure 6. The Normalized Transmitted Fields H(t, d)/H_0 as Functions of Time for Different Incident Amplitudes for a Non-Linear μ_R(H)

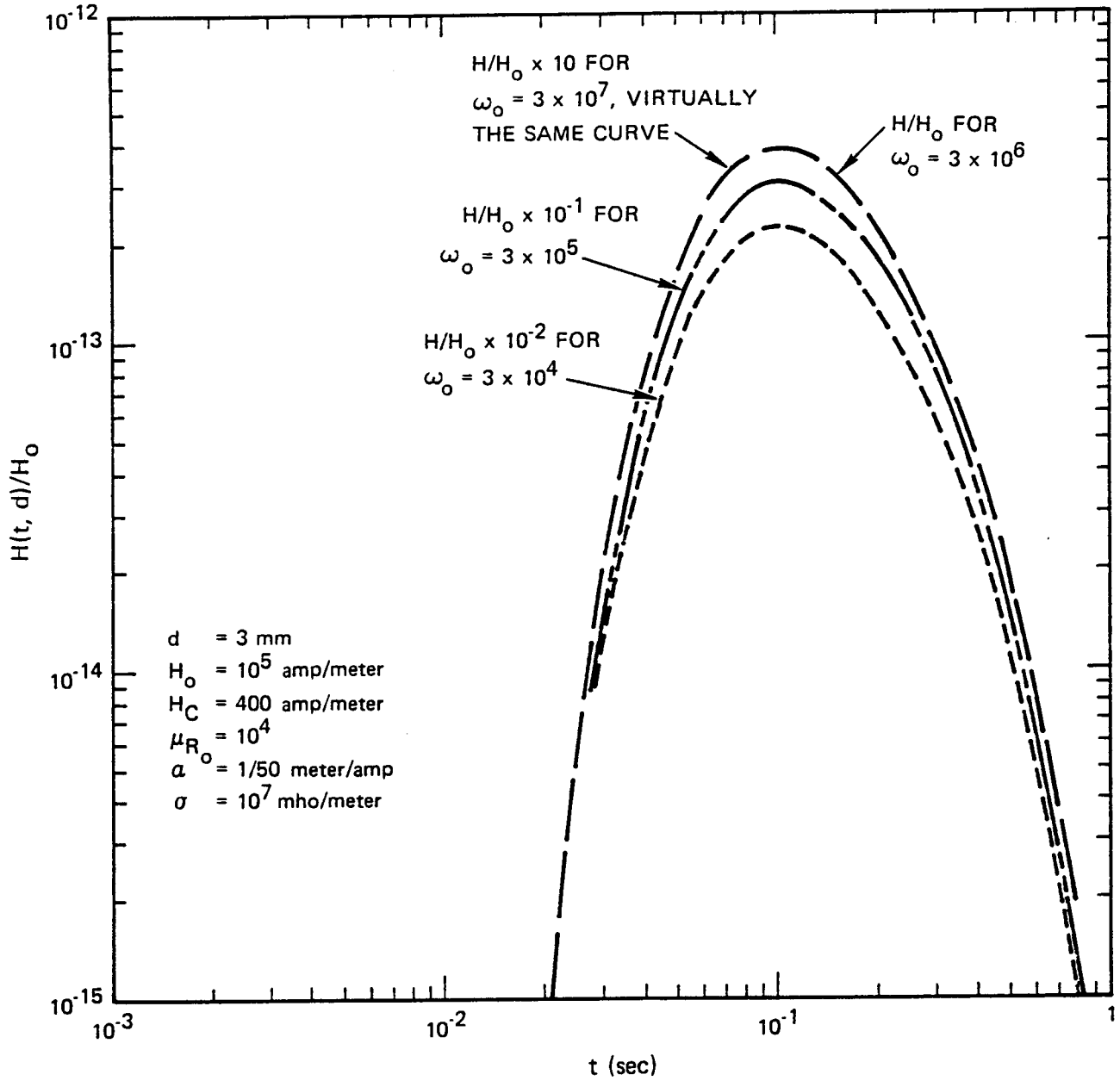

Figure 7. The Normalized Transmitted Magnetic Fields $H(t, d)/H_o$ as Functions of Time for Different $\omega_o \equiv \pi/T_o$, for a Non-Linear $\mu_R(H)$

give similar results (Figure 7). Fourth, under these same conditions but varying the slab thickness d (Figure 8) and the $\mu_{Ro} \equiv \mu_R(0)$ (Figure 9), respectively, in the typical nonlinear example shows a time scaling proportional to $\mu_{Ro} d^2$, and an amplitude dependence approximately as $\sim \mu_{Ro}^{-1} d^3$ but slightly less than such a scaled value. Again, this is expected from (22) and Section 2.2.1.

We conclude this numerical section by stating again that for short pulses and thick slabs, under condition (23), (28), and (29), the transmitted magnetic field for the nonlinear μ obeys approximately (22), with $\mu_r = \mu_{Ro}$, but becomes slightly smaller as corrected by (30).

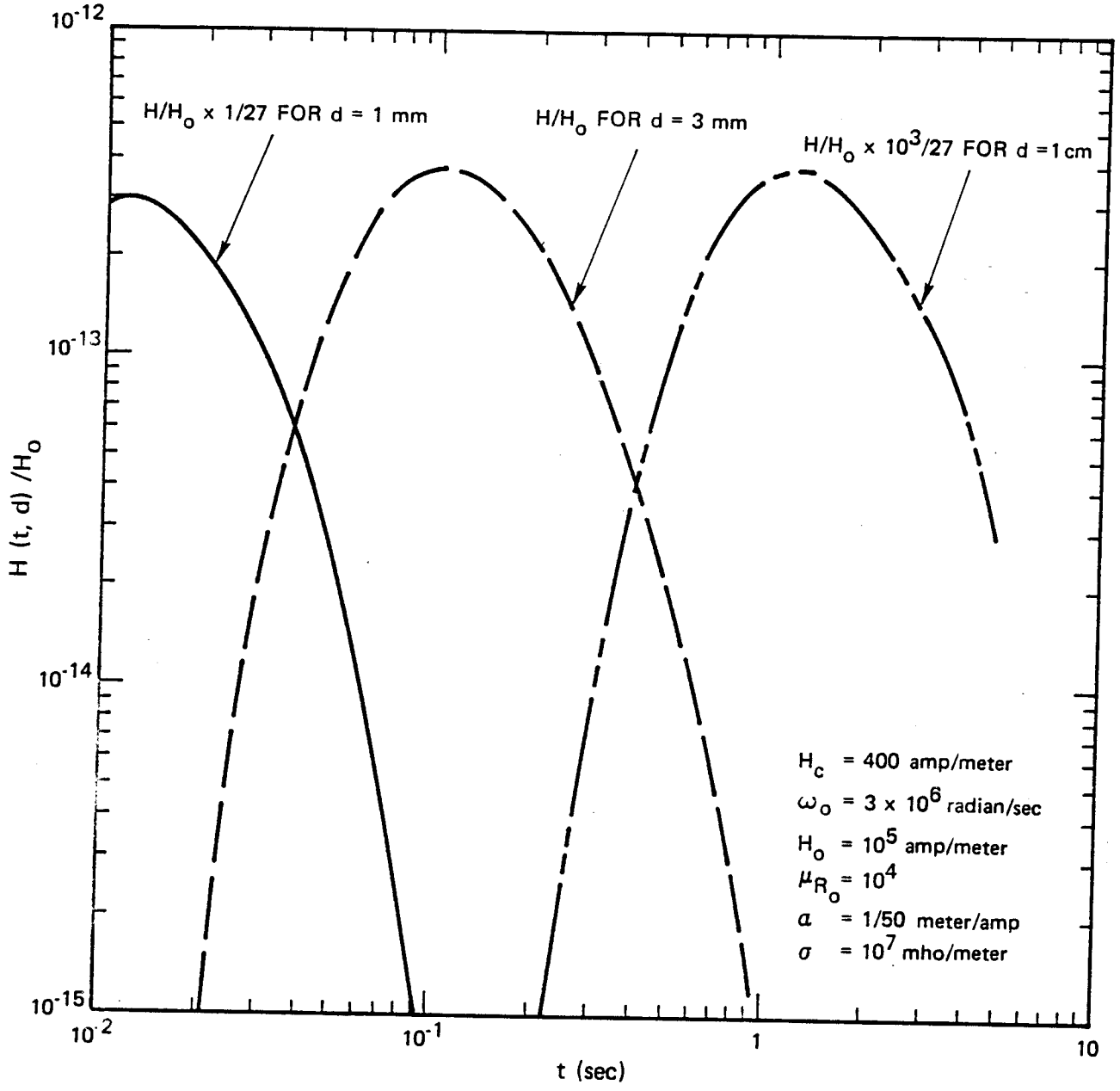

Figure 8. The Transmitted Magnetic Fields $H(t, d)/H_o$ as Functions of Time for Different Slab Thickness d, for a Non-Linear $\mu_R(H)$

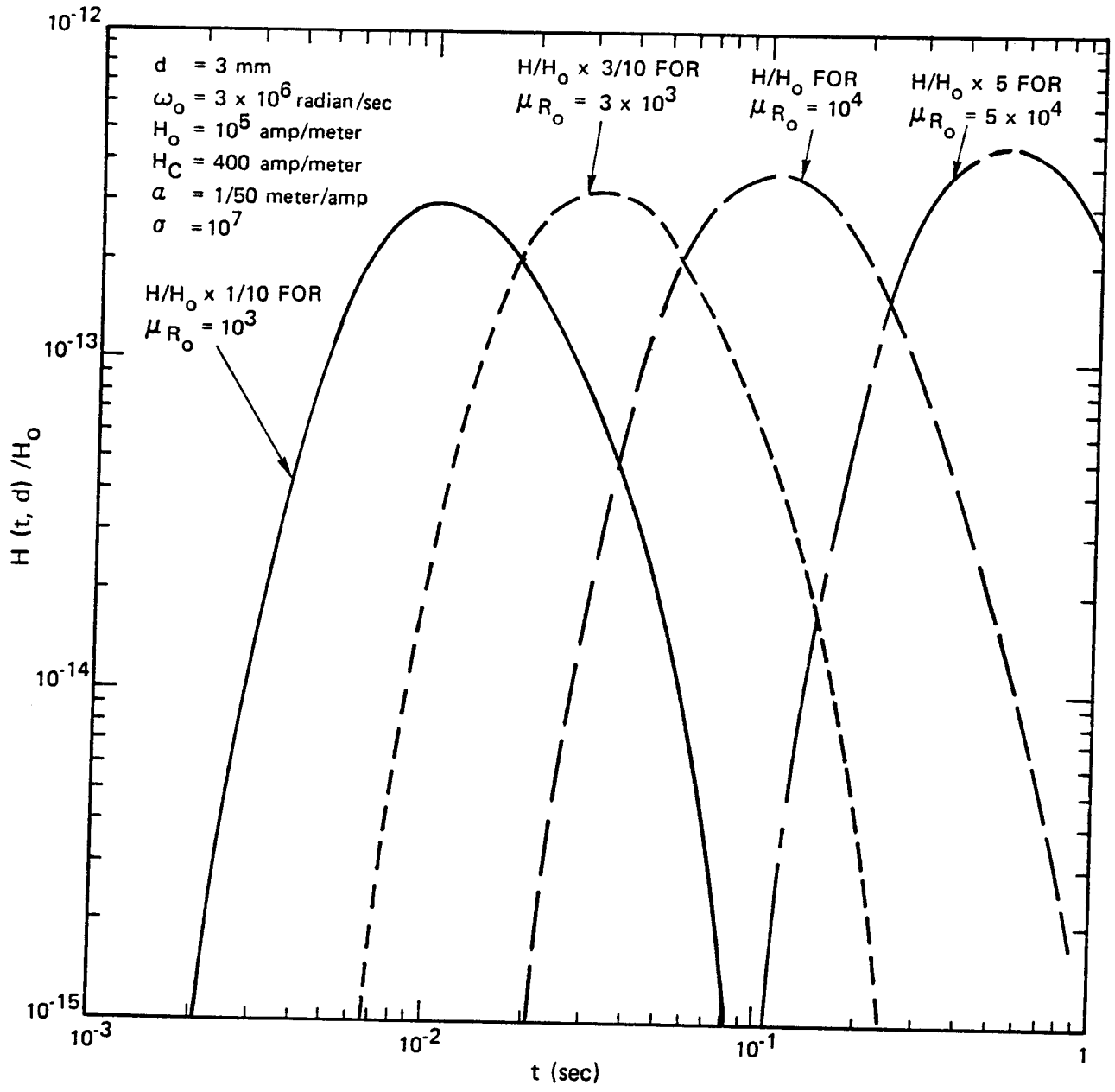

Figure 9. Transmitted Magnetic Fields H(t, d)/H_o as Functions of Time for Different μ_{R_o}, for a Non-Linear μ_R(H)

SECTION 3. THE CYLINDRICAL-INCIDENCE SLAB PROBLEM

Consider Figure 10, an incident cylindrical TEM wave

$$H_{\phi}^{in}(t,\rho,z) = \frac{I_o}{2\pi\rho} f\left(t - \frac{z}{c}\right) \tag{33a}$$

$$E_{\rho}^{in}(t,\rho,z) = \frac{I_o}{2\pi\rho}\sqrt{\frac{\mu_o}{\epsilon_o}} f\left(t - \frac{z}{c}\right) \tag{33b}$$

carrying a z-flowing current $I_o f(t - z/c)$ on the surface of a perfectly conducting wire of radius a impinging upon a slab as shown. In the cylindrical coordinates (ρ,ϕ,z), the ϕ-symmetry makes fields functions of (t,ρ,z). The parameters in Figure 10 have the same meanings as in Figure 1.

Before solving the problem, we must make several remarks here. First, one can, of course, solve the problem numerically either by finitely differencing the field equations subject to the boundary conditions or by finitely patching the perfect-conductor mixed surface integral equations to solve for the surface current density on the wire and then to obtain the field from the surface current density. Second, with its end surface present the semi-infinite cylinder does not have its surface as one of the coordinate surfaces of the eleven coordinate systems that permit the separation of variables for the Helmholtz equation. Thus in using the familiar method of solving by the separation of variables and summation of the products of the eigen functions (in this case the Hankel transform for ρ or the (2-sided) Laplace transform for z), not only are the coefficients mixed by the boundary conditions but also the expansion does not converge at the edge of the cylindrical end where the electric field goes to infinity (although weakly if edge condition of finite energy is imposed). But to match boundary conditions means that we would have to manipulate and evaluate the coefficients of a series at precisely the place where the series representation is not valid. As a result, no consistent solution can possibly be obtained by such a familiar method. The rigorous analytical

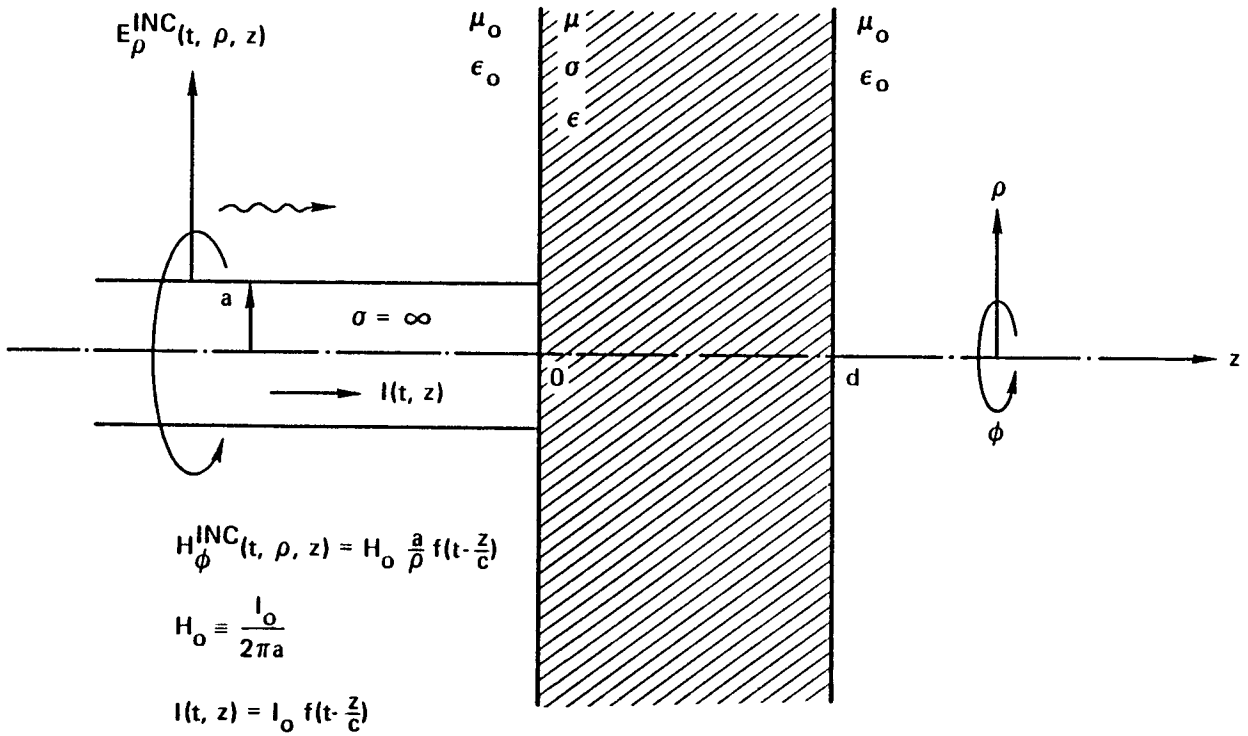

Figure 10. Cylindrical Diffusion Problem

solution, even to the simplified problem without the presence of the slab, is therefore still an unanswered question [8].

In the following, we solve the cylindrical-incidence problem by an approximate method whose validity range is established to be of practical interest. The resulting formulas, being simply related to those for the one-dimension problem, enable us to make use of results in Section 2 for the present cylindrical problem.

3.1 ANALYSIS FOR THE CONSTANT μ CASE

To find the diffused fields and the transmitted fields in $z > 0$, the only physical quantity we really need from the incident $z < 0$ side is the tangential field, either electric or magnetic, at $z = 0$. Although it does not matter which one we start with if we can solve the problem exactly, it does make a difference in solving the problem approximately depending on which approximation can be made more easily and more accurately.

Now, for the real problem both the "wire region" $\rho < a$, $z < d$ and the "surrounding slab region" $\rho \geq a$, $0 < z < d$ are highly conducting. The magnetic field at the "inside" boundary $\rho \lesssim a-\delta_w$, $z = 0$, where δ_w is the skin depth of the wire region and is $<< a$, is clearly much smaller than the H_ϕ at the "outside" boundary $\rho \gtrsim a$, $z = 0$, regardless of the existence of the conducting surrounding slab. In fact, without the slab's presence this has been used to justify the incident current I_o being associated to a cylindrical TEM wave outside the wire, and with the slab's presence, and reflection, this is even more pronounced. Moreover, the area of the "inside" boundary, $\sim a^2$, is much smaller than the area of the "outside" boundary, ∞. This makes the diffused and transmitted fields, being the surface integration of the cross product of the $H_\phi \underset{\sim}{e}_\rho$ and the gradient of the Green's function, depend even less on the "inside" magnetic field. Thus, the H_ϕ at the "outside" boundary alone predominatly determines the diffused and transmitted fields. However, a similar result does not hold

for the boundary electric field. Because the "inside" boundary electric field E_ρ, though negligibly small relative to the "outside" boundary one when there exists no conducting surrounding slab, is not comparatively negligibly small when the conducting surrounding slab is present and makes the "outside" boundary E_ρ also vanishingly small. Consequently, we must use the magnetic matching, not the electric matching, if we use the "outside" boundary fields only as an approximation.

Finally, for the case of narrow incident pulse and thick slab of practical interest ((28) & (29)), the approximate "outside" boundary magnetic field can be found easily. Since the slab makes the H_ϕ at $\rho > a$, $z = 0$ not sensitive to the geometry beyond $z > d$, the H_ϕ there is virtually unchanged if we extend the wire beyond $z = d$ to $z = \infty$. Furthermore, since the wire is itself highly conducting, as far as fields on it are concerned we can replace it by a perfectly conducting wire. The following analysis follows such an approximation procedure.

3.1.1 Formulation and Analysis

If the perfectly conducting wire extends to all z, then the incident TEM wave (33) produces only TEM waves. Their wave forms for a constant μ slab are just the one-dimensional results with H_o replaced by $H_o a/\rho$ where $H_o = I_o/(2\pi a)$, and with E_x and H_y substituted by E_ρ and H_ϕ respectively. In particular, from (11)

$$\hat{H}_\phi^{(\infty \text{ wire})}(s,\rho,0) = \frac{I_o}{2\pi\rho} \cdot \frac{2\hat{f}(s)\left[(1+\alpha) - (1-\alpha)e^{-2\sqrt{\mu\sigma s}\, d}\right]}{(1+\alpha)^2 - (1-\alpha)^2 e^{-2\sqrt{\mu\sigma s}\, d}}, \quad \rho > a$$

$$= 0, \quad \rho < a \tag{34}$$

where $\alpha \equiv (\mu_r \varepsilon_o s/\sigma)^{1/2}$.

Now, for the real problem of a terminated wire with ϕ-symmetry, the TEM wave cannot exist in the region $z > 0$ because of its necessarily accompanying singularity at $\rho = 0$. Further, a TE wave, under the condition $\partial/\partial\phi \equiv 0$, has only E_ϕ^{TE}, H_ρ^{TE}, and H_z^{TE} as the non-vanishing components. But the boundary conditions, the continuity of tangential fields at $z = 0$ and $z = d$, do not couple this TE mode to the incident TEM wave at all. Thus the TE wave has its existence independent of the incident wave and can be taken as identically zero. Finally, a TM wave does exist, with non-vanishing components H_ϕ^{TM}, E_ρ^{TM}, and E_z^{TM}. In $z > 0$, this is the only mode existing, and its superscripts are omitted in the following.

Similar to the one-dimension problem, the diffused fields in the highly conducting slab $0 < z < d$ satisfy (2) and obey the equations

$$\sigma E_\rho = -\frac{\partial}{\partial z} H_\phi \tag{35a}$$

$$\sigma E_z = \frac{1}{\rho}\frac{\partial}{\partial \rho}(\rho H_\phi) \tag{35b}$$

$$\frac{\partial^2 H_\phi}{\partial \rho^2} + \frac{1}{\rho}\frac{\partial}{\partial \rho} H_\phi - \frac{H_\phi}{\rho^2} + \frac{\partial^2 H_\phi}{\partial z^2} - \mu\sigma \frac{\partial H_\phi}{\partial t} = 0 \tag{35c}$$

In $z > d$ they obey similar equations as (35) but with σ replaced by $\varepsilon_o \partial/\partial t$. To solve the problem, in addition to the Laplace transform in time we make use of the Hankel transform in ρ [9].

$$\psi(\rho) = \int_0^\infty dK\, J_\nu(K\rho)\tilde{\psi}(K), \quad \rho > 0 \tag{36}$$

Now, requiring as usual a + z traveling wave in $z > d$, finite fields at $\rho = 0$, continuous E_ρ and H_ϕ at $z = d$, and that $\hat{H}_\phi(s,\rho,0) = \hat{H}^{(\infty \text{ wire})}(s,\rho,0)$ of (34), the magnetic field in $0 < z < d$ is (Appendix G)

$$\hat{H}_\phi(s,\rho,z) = \int_0^\infty dK\, J_1(K\rho)\left[\xi(K,s)e^{-K_>z} + \eta(K,s)e^{K_>z}\right] \tag{37}$$

where

$$\begin{pmatrix}\xi(K,s)\\ \eta(K,s)\end{pmatrix} = \frac{q(K,s)\begin{pmatrix}(1+\beta)e^{K_>d}\\ -(1-\beta)e^{-K_>d}\end{pmatrix}}{e^{K_>d}(1+\beta) - e^{-K_>d}(1-\beta)} \tag{38}$$

and

$$q(K,s) \equiv \frac{I_o J_o(Ka)\hat{f}(s)}{\pi} \cdot \frac{(1+\alpha) - (1-\alpha)e^{-2\sqrt{\mu\sigma s}\,d}}{(1+\alpha)^2 - (1+\alpha)^2 e^{-2\sqrt{\mu\sigma s}\,d}} \tag{39a}$$

$$\beta \equiv \frac{s\varepsilon_o K_>}{\sigma K_<} \tag{39b}$$

$$K_> \equiv \sqrt{K^2+\mu\sigma s} \quad , \quad \text{Real}\{K_>\} > 0 \quad , \tag{39c}$$

$$K_< \equiv \sqrt{K^2+\mu_o\varepsilon_o s^2} \quad , \quad \text{Real}\{K_<\} > 0 \tag{39d}$$

The electric fields in $0 < z < d$ are given immediately by (37) and (35a,b) The fields in $z > d$ are (Appendix G)

$$\hat{H}_\phi(s,\rho,z) = s\varepsilon_o\int_0^\infty dK\, Kp(K,s)J_1(K\rho)e^{-K_<(z-d)} \tag{40a}$$

$$\hat{E}_\rho(s,\rho,z) = \int_0^\infty dK\, KK_<p(K,s)J_1(K\rho)e^{-K_<(z-d)} \tag{40b}$$

$$\hat{E}_z(s,\rho,z) = \int_0^\infty dK\, K^2p(K,s)J_o(K\rho)e^{-K_<(z-d)} \tag{40c}$$

where

$$p(K,s) = \frac{q(K,s)}{s\varepsilon_o K} \cdot \frac{2\beta}{e^{K_>d}(1+\beta) - e^{-K_>d}(1-\beta)} \tag{41}$$

3.1.2 Results and Their Relations to the One-Dimension Problem

For a highly conducting ($\alpha << 1$, condition (13)) thick ($\sigma d\sqrt{\mu_o/\varepsilon_o} >> 1$, condition (23))slab, ξ, η, and p reduce to (Appendix G)

$$\begin{pmatrix} \xi(K,s) \\ \eta(K,s) \end{pmatrix} = \frac{I_o J_o(Ka)\hat{f}(s)}{2\pi Sh(K_> d)} \begin{pmatrix} e^{K_> d} \\ -e^{-K_> d} \end{pmatrix} \tag{42}$$

$$p(K,s) = \frac{I_o J_o(Ka)\hat{f}(s) K_>}{\pi\sigma K K_< Sh(K_> d)} \tag{43}$$

We examine next such cases in detail.

From (40b), (41), and (43), the transmitted radial electric field at $z = d$ is (Appendix H)

$$E_\rho(t,\rho,d) = \frac{I_o}{\pi\sigma d}\int_0^\infty dt' f(t-t')\left[\frac{d}{dt'}\,\theta_4\left(0\middle|\frac{i\pi t'}{\mu\sigma d^2}\right)\right]\int_0^\infty dK J_1(K\rho)J_o(Ka)e^{\frac{-K^2 t'}{\mu\sigma}}$$

$$\sim \frac{I_o}{\pi\sigma d}\int_0^\infty dt' f(t-t')\left[\frac{d}{dt'}\,\theta_4\left(0\middle|\frac{i\pi t'}{\mu\sigma d^2}\right)\right]\cdot\frac{1-e^{\frac{-\mu\sigma\rho^2}{4t'}}}{\rho} \tag{44a}$$

$$\text{if } \rho >> \min\left(a,\sqrt{\frac{t'}{\mu\sigma}}\right) \tag{44b}$$

$$\sim \frac{I_o}{\pi\sigma d}\int_0^\infty dt' f(t-t')\left[\frac{d}{dt'}\,\theta_4\left(0\middle|\frac{i\pi t'}{\mu\sigma d^2}\right)\right]\cdot\frac{\mu\sigma\rho}{4t'}\,e^{\frac{-\mu\sigma a^2}{4t'}}$$

$$\text{if } \rho << \max\left(a,\sqrt{\frac{t'}{\mu\sigma}}\right) \tag{44c}$$

and becomes

$$E_\rho^{(\delta)}(t,\rho,d) = \frac{2a}{\sigma d}\left[\frac{d}{dt}\,\theta_4\left(0\middle|\frac{i\pi t}{\mu\sigma d^2}\right)\right]\int_0^\infty dK\, J_1(K\rho)J_o(Ka)e^{\frac{-K^2 t}{\mu\sigma}} \tag{45a}$$

$$\sim \frac{2a}{\sigma d}\left[\frac{d}{dt}\,\theta_4\left(0\middle|\frac{i\pi t}{\mu\sigma d^2}\right)\right]\cdot\frac{1-e^{\frac{-\mu\sigma\rho^2}{4t}}}{\rho},$$

$$\text{if } \rho >> \min\left(a,\sqrt{\frac{t}{\mu\sigma}}\right) \tag{45b}$$

$$\sim \frac{2a}{\sigma d}\left[\frac{d}{dt}\,\theta_4\left(0\middle|\frac{i\pi t}{\mu\sigma d^2}\right)\right]\cdot\frac{\mu\sigma\rho}{4t}\,e^{\frac{-\mu\sigma\rho^2}{4t}},$$

$$\text{if } \rho << \max\left(a,\sqrt{\frac{t}{\mu\sigma}}\right) \tag{45c}$$

for a δ-incidence $H^{inc}(t,\rho,z) = \delta(t-z/c)a/\rho$. Here $\theta_4(v|\tau)$ is one of the Theta functions [10].

Similarly, from (40a) the transmitted magnetic field is

$$H_\phi(t,\rho,d) = \sqrt{\frac{\varepsilon_o}{\mu_o}}\,E_\rho(t,\rho,d) + H_{\phi,dev}(t,\rho,d) \tag{46}$$

Here, $H_{\phi,dev}(t,\rho,d)$ is the part of magnetic field which deviates (in its relation to E_ρ) from that of a pure TEM wave (Appendix H)

$$H_{\phi,dev}(t,\rho,d) = \frac{-I_o}{\pi\sigma d\mu_o}\int_0^t dt'\int_0^{t-t'} dt''f(t-t'-t'')\left[\frac{d}{dt''}\,\theta_4\left(0\middle|\frac{i\pi t''}{\mu\sigma d^2}\right)\right]$$
$$\int_0^\infty dK\, KJ_1\left(\frac{Kt'}{\sqrt{\mu_o\varepsilon_o}}\right)J_o(Ka)J_1(K\rho)e^{\frac{-K^2t''}{\mu\sigma}} \tag{47a}$$

$$\sim \frac{-I_o \mu_r}{2\pi d} \int_0^t \frac{dt''}{t''} \int_0^{t-t''} dt' \; f(t-t'-t'') \left[\frac{d}{dt''} \theta_4\left(0 \middle| \frac{i\pi t''}{\mu\sigma d^2}\right)\right]$$

$$e^{\frac{-\mu\sigma(\rho^2+c^2t'^2)}{4t''}} \; I_1\left(\frac{\mu\sigma c\rho t'}{2t''}\right)$$

$$\text{if } a << \max(\rho, ct') \tag{47b}$$

$$\sim \frac{-I_o}{\pi\sigma d\mu_o} \int_0^t dt'' \int_0^{t-t''} dt' \; f(t-t'-t'') \left[\frac{d}{dt''} \theta_4\left(0 \middle| \frac{i\pi t''}{\mu\sigma d^2}\right)\right]$$

$$\frac{\rho t'}{4\sqrt{\mu_o \varepsilon_o}} \left(\frac{\mu\sigma}{2t''}\right)^3 e^{\frac{-\mu\sigma a^2}{4t''}} \left(\frac{4t''}{\mu\sigma} - a^2\right)$$

$$\text{if } a >> \max(\rho, ct') \tag{47c}$$

and its δ-response becomes

$$H^{(\delta)}_{\phi,\text{dev}}(t,\rho,d) = \frac{2a}{\sigma d\mu_o} \int_0^t dt'' \int_0^{t-t''} dt' \left[\frac{d}{dt} \theta_4\left(0 \middle| \frac{i\pi t''}{\mu\sigma d^2}\right)\right] \int_0^\infty dK$$

$$KJ_1\left(\frac{K(t-t'')}{\sqrt{\mu_o\varepsilon_o}}\right) J_o(Ka) J_1(K\rho) e^{\frac{-K^2 t''}{\mu\sigma}} \tag{48a}$$

$$\sim -\sqrt{\frac{\varepsilon_o}{\mu_o}} \; \frac{2a}{\sigma d} \left[\frac{d}{dt} \theta_4\left(0 \middle| \frac{i\pi t}{\mu\sigma d^2}\right)\right] e^{\frac{-\mu\sigma\rho^2}{4t}} \quad \frac{\mu\sigma\rho}{4t}$$

$$\text{if } \rho >> a, \; e^{\mu\sigma c^2 t/4} >> 1, \tag{48b}$$

$$\sim -\sqrt{\frac{\varepsilon_o}{\mu_o}} \; \frac{2a}{\sigma d} \left[\frac{d}{dt} \theta_4\left(0 \middle| \frac{i\pi t}{\mu\sigma d^2}\right)\right] e^{\frac{-\mu\sigma a^2}{4t}} \; \frac{\mu\sigma\rho}{4t} \; \frac{\mu\sigma a^2}{4t},$$

$$\text{if } \rho << a \tag{48c}$$

Thus at large ρ and small ρ the total magnetic fields, respectively, are

$$H_{\phi}^{(\delta)}(t,\rho,d) \sim \frac{2a}{\sigma d}\left[\frac{d}{dt}\,\theta_4\left(0\middle|\frac{i\pi t}{\mu\sigma d^2}\right)\right]\sqrt{\frac{\varepsilon_o}{\mu_o}}\;\frac{1 - e^{(-\mu\sigma\rho^2)/(4t)}\left(1 + \frac{\mu\sigma\rho^2}{4t}\right)}{\rho}$$

$$\text{if } \rho >> a,\ e^{(\mu\sigma\rho^2 t)/4} >> 1, \tag{49a}$$

$$\sim \frac{2a}{\sigma d}\left[\frac{d}{dt}\,\theta_4\left(0\middle|\frac{i\pi t}{\mu\sigma d^2}\right)\right]\sqrt{\frac{\varepsilon_o}{\mu_o}}\;\frac{\mu\sigma\rho}{4t}\left[e^{(-\mu\sigma\rho^2)/(4t)} + e^{(-\mu\sigma a^2)/(4t)}\,\frac{\mu\sigma a^2}{4t}\right]$$

$$\text{if } \rho << a \tag{49b}$$

for a $H^{inc}(t,\rho,z) = \delta(t - \frac{z}{c})\ a/\rho$.

Comparing (45) to (49) with the one-dimension results (4) and (19), we see that

$$H_{\phi}^{(\delta)}(t,\rho,d) \sim H_{one\text{-}D}^{(\delta)}(t,d)\ \frac{a}{\rho}\left[1 - e^{(-\mu\sigma\rho^2)/(4t)}\ \left(1 + \frac{\mu\sigma\rho^2}{4t}\right)\right]$$

$$\text{if } \rho >> a,\ e^{(\mu\sigma c^2 t)/4} >> 1 \tag{50a}$$

$$\sim H_{one\text{-}D}^{(\delta)}(t,d)\ \frac{\rho}{a}\,\frac{\mu\sigma a^2}{4t}\,e^{(-\mu\sigma\rho^2)/(4t)}$$

$$\left[1 + e^{-[\mu\sigma(a^2-\rho^2)]/4}\,\frac{\mu\sigma a^2}{4t}\right]$$

$$\text{if } \rho << a \tag{50b}$$

and

$$E^{(\delta)}(t,\rho,d) = E^{(\delta)}_{one\text{-}D}(t,d)\ \frac{a}{\rho}\left[1 - e^{-\mu\sigma\rho^2/(4t)}\right]$$

$$\text{if } \rho >> \min\left(a, \sqrt{\frac{t}{\mu\sigma}}\right) \tag{51a}$$

$$= E^{(\delta)}_{one\text{-}D}(t,d)\ \frac{\rho}{a}\ \frac{\mu\sigma a^2}{4t}\ e^{(-\mu\sigma\rho^2)/(4t)}$$

$$\text{if } \rho << \max\left(a, \sqrt{\frac{t}{\mu\sigma}}\right) \tag{51b}$$

The relations (50a) and (51a) for large $\rho >> a$ are intuitively plausible: at early times before the effect of the wire region diffuses there, $t << \mu\sigma\rho^2/4$, the fields do not feel the termination of the wire and are just the diffused cylindrical TEM wave with the one-dimensional fields multiplied by a/ρ, and at later time, the fields become smaller than such a TEM version because they diffuse into the wire region. The normalized ratios $H^{(\delta)}_{\phi}(t,\rho,d)/(H^{(\delta)}_{one\text{-}D}(t,d)\ a/\rho)$ and $E^{(\delta)}_{\rho}(t,\rho,d)/(E^{(\delta)}_{one\text{-}D}(t,d)\ a/\rho)$ as functions of a normalized time $X = t/(\mu\sigma\rho^2)$ show (Figure 11) such behaviors. The one-dimensional peak diffused-through time $X_{pk/d} = t_{pk/d}/(\mu\sigma\rho^2)$ (see (22b)) as a function of d/ρ shows (Figure 11) that for $d/\rho \lesssim 1$ the diffused fields are virtually a pure cylindrical TEM wave up to the peak.

For small $\rho << a$, the $H^{(\delta)}_{\phi}(t,\rho,d)$ and $E^{(\delta)}_{\rho}(t,\rho,d)$ given respectively by (50b) and (51b) go to zero at least as fast as ρ, a consistent behavior with a finite E_z and a finite total (conducting and displacement) current density near $\rho = 0$, and, of course, start from zero at $t = 0$. The ratios $H^{(\delta)}_{\phi}(t,\rho,d)/H^{(\delta)}_{one\text{-}D}(t,d)$ and $E^{(\delta)}_{\rho}(t,\rho,d)/E^{(\delta)}_{one\text{-}D}(t,d)$ show such behaviors (Figures 12-1, 12-2, plotted similarly to Figure 11 but with ρ replaced by a for the normalized time $t/(\mu\sigma a^2)$ and with ρ as a parameter).

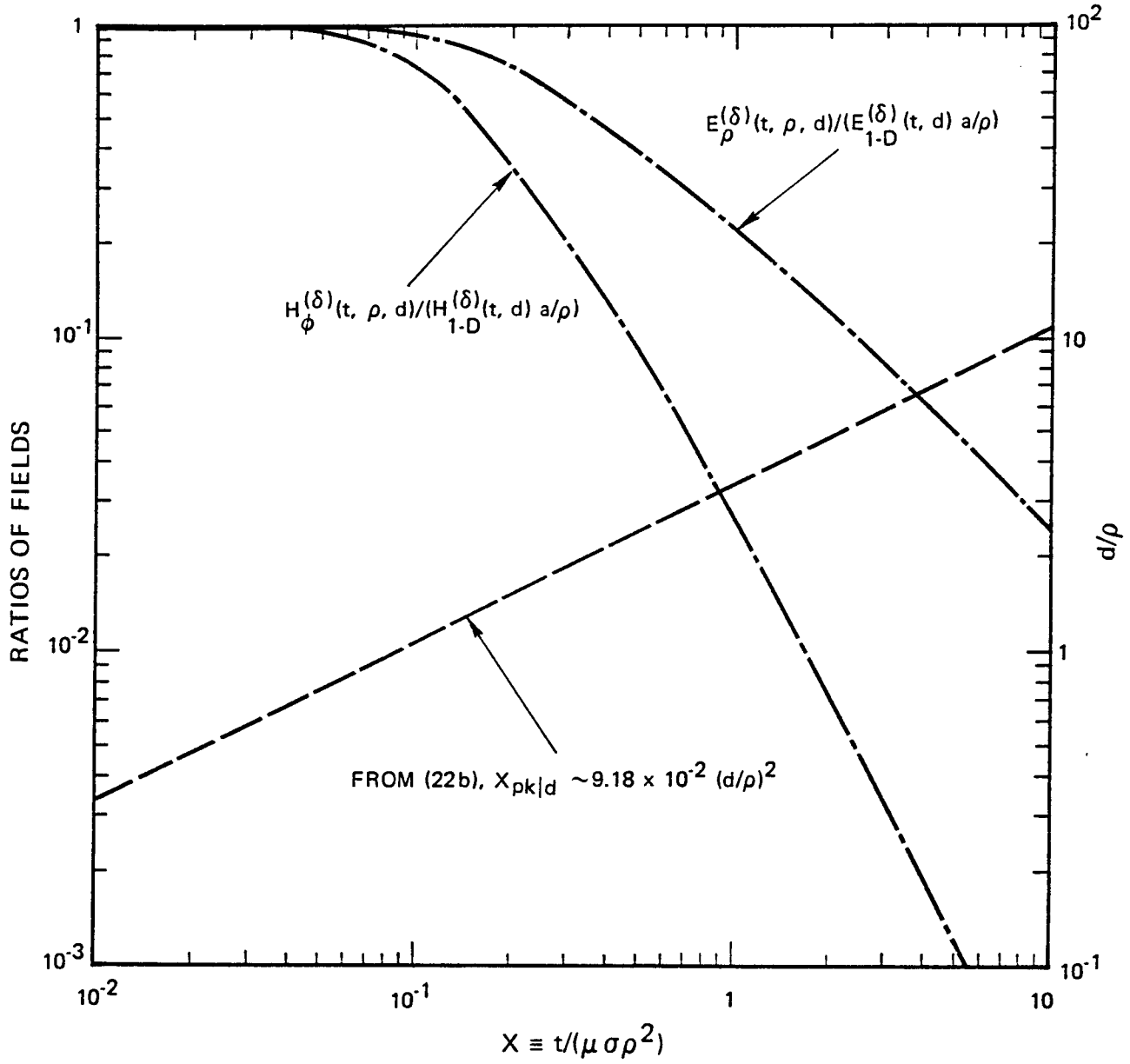

Figure 11. The Normalized Ratios $H_\phi^{(\delta)}(t, \rho, d)/(H_{1\text{-}D}^{(\delta)}(t, d)\frac{a}{\rho})$ and $E_\rho^{(\delta)}(t, \rho, d)/(E_{1\text{-}D}^{(\delta)}(t, d)\frac{a}{\rho})$ from the $\rho \gg a$ Expressions (50-a) and (51-a) as Functions of Normalized Time $t/(\mu\sigma\rho^2)$, and the Normalized 1-D Peak Time $X_{pk|d} = t_{pk|d}/(\mu\sigma\rho^2)$ as a Function of (d/ρ)

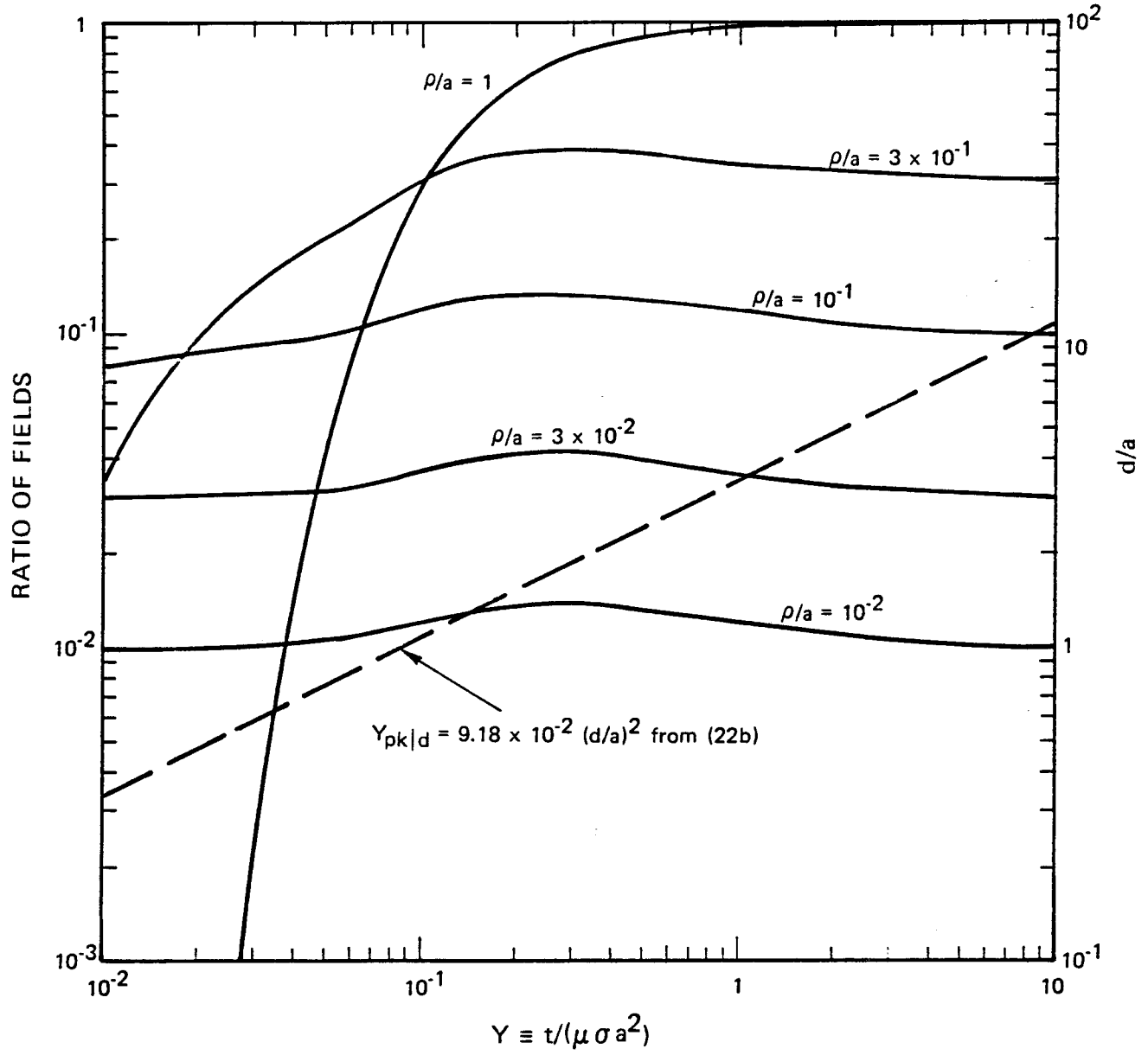

Figure 12-1. The Ratios $H_{\phi}^{(\delta)}(t, \rho, d)/H_{1-D}^{(\delta)}(t, d)$ from the $\rho \ll a$ Expression (50b) as Functions of Normalized Time $t/(\mu\sigma a^2)$ and the Normalized 1-D Peak Time $Y_{pk|d} = t_{pk|d}/(\mu\sigma a^2)$ as a Function of (d/a)

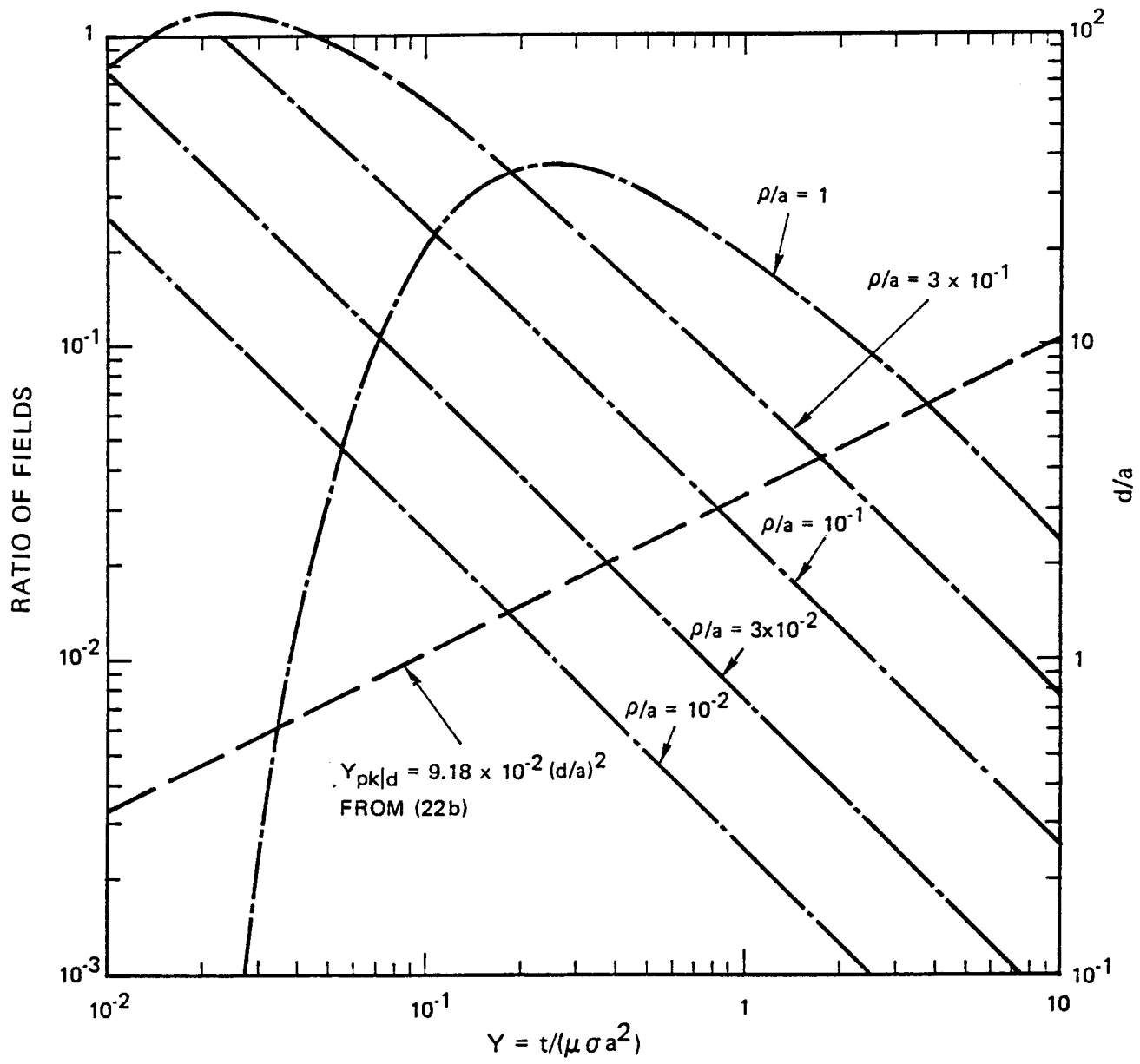

Figure 12-2. The Ratio $E_{\rho}^{(\varepsilon)}(t, \rho, d)/E_{1-D}^{(\delta)}(t, d)$ from the $\rho \ll a$ Expression (51b) as Functions of the Normalized Time $t/(\mu\sigma a^2)$, and the Normalized 1-D Peak Time $Y_{pk|d} = t_{pk|d}/(\mu\sigma a^2)$ as a Function of (d/a)

Now consider $\rho \sim a$. From (45b), the $E_\rho^{(\delta)}(t,\rho>>a,d)$ expression is also valid for $E_\rho^{(\delta)}(t<<\mu\sigma a^2,\rho\sim a,d)$. Similarly from (45c), the expression $E_\rho^{(\delta)}(t,\rho<<a,d)$ is valid for $E_\rho^{(\delta)}(t>>\mu\sigma a^2,\rho\sim a,d)$. Thus, for $\rho = a$, the ratio $E_\rho^{(\delta)}(t,a,d)/E_{one-D}^{(\delta)}(t,d)$ at early times $t << \mu\sigma a^2$ is given by the large ρ curve (the E-curve, $X << 1$ part in Figure 11 with $\rho = a$) and at late times $t >> \mu\sigma a^2$ is given by the small ρ curve (the $Y >> 1$ part of the $\rho = a$ curve in Figure 12-2). At $t \sim \mu\sigma a^2$, they do join smoothly at ~ 0.2 (the E-curve at $X \sim 1$ in Figure 11 and the $\rho/a = 1$ curve at $Y \sim 1$ in Figure 12-2) which should be the right value. Similar conclusions hold for the $H_\phi^{(\delta)}(t,\rho\sim a,d)/H_{one-D}^{(\delta)}(t,d)$. This is because at $\rho \sim a$ the part of magnetic field which diverts (see (46)) from the TEM-like behavior is negligible for early times and for late times, respectively, in the large ρ expression (50a) and in the small ρ expression (50b).

We conclude by restating that (50) and (51) (plotted in Figures 11,12) are valid relations between the cylindrical and the one-dimensional solutions for highly conducting thick slabs of practical interest. From these relations, we can multiply the one-dimension fields obtained in Section 2 by a cylindrical-effect factor to make predictions for the cylindrical-incidence problem.

3.2 THE NONLINEAR μ CASE

The nonlinear saturation effect can only occur in a region

$$a \sim \rho \lesssim \frac{H_o}{H_c} a \tag{52}$$

From Section 2.2 we have found that for the practically interesting cases of highly conducting thick slabs with narrow incident pulses (conditions (23), (28), (29)), saturation only reduces slightly the transmitted fields but leaves intact their time shapes. Such are the effects the cylindrical transmitted fields in region (52) will experience,

with (50) and (51) still being the formulas to relate to those of the one-dimension nonlinear problem which are solved semi-analytically or numerically.

For ρ not in the region (52), the constant-μ results in Section 3.1 apply directly.

Finally, we shall conclude with an example. Consider the typical problem in Section 2.2.2, but with a wire of radius $\sim$0.5 cm carrying an incident $I_o = 2\pi\, aH_o = 3.14 \times 10^3$ amp. The transmitted magnetic field in the region $\rho \lesssim 1.25$ m is approximately the $H_o = 10^5$ amp/m curve in Figure 6 multiplied by the cylindrical factors (50) or its plots (Figures 11, 12--1). For example, at $\rho \sim a$, the transmitted field has a peak value

$$H_\phi(t_{pk/d}, \rho \sim a, d) \sim \underbrace{10^5}_{H_o} \times \underbrace{3.8 \times 10^{-13}}_{\substack{\text{one-D} \\ \text{from} \\ \text{Figure 6}}} \times \underbrace{1.0}_{\substack{\text{at } X_{pk/d} \\ \text{from} \\ \text{Figure} \\ 11}} \times \underbrace{\frac{1}{1}}_{\frac{\rho}{a}=1} \sim 3.8 \times 10^{-8} \text{ amp/m}$$

with a peak diffusion time $\sim 1.1 \times 10^{-1}$ sec and a diffused pulse width $(\Delta t)_{1/10} \sim 4.0 \times 10^{-1}$ sec, same as for the one-dimensional case. For $\rho > a$, the peak field is smaller by a factor $\sim a/\rho$, but that factor approaches $\sim (0.8)^{-1} a/\rho$ as $\rho >> 1.25$ m. At $\rho < a$, the peak decreases from (53) at $\rho \sim a$ to zero at $\rho = o$, roughly proportional to ρ as $\rho \lesssim a$ and according to (50b) as $\rho << a$.

FOOTNOTES AND REFERENCES

1. For the general EMP generation mechanism and pulse shapes, see the beginning part of this special issue. For some early work, see e.g. W. J. Karzas, R. Latter, Phy. Rev., 126, 1919 (June 1962); 137, B 1369 (March 1965); also J. Geoph. Research, 67, 4635 (Nov 1962); C. L. Longmire, "Theory of the EMP from Nuclear Surface Burst," LANC-R-6, Los Alamos Nuclear Corp. (1970).

2. The subject of shielding has drawn many efforts since long ago. See any textbook in EM theory, e.g., J. A. Stratton, Electromagnetic Theory (McGraw-Hill, 1941), for a simple description of the shielding effect and for the EM theory used in this paper. For some recent EMP shielding, see the many papers included in the EMP notes, AFWL, edited by C. E. Baum; e.g., C. W. Harrison, Jr., M. L. Houston, R. W. P. King, T. T. Wu, "The Propagation of Transient EM Fields into a Cavity Formed by Two Imperfectly Conducting Sheets," (April 1964, Sandia Corp. Rept.). AFWL-EMP-3-2-#31 (1971); C. W. Harrison, Jr., C. H. Papas, "On the Attenuation of Transient Fields by Imperfectly Conducting Spherical Shells," (July 1964, Sandia Corp. Rept.) AFWL-EMP-3-2-#34 (1971); K. S. H. Lee, "Shields With Periodic Aperatures," (Jan 1972, Northrop Corp. Labs. Rept.) AFWL-EMP-3-2-#89.

3. Numerous works have been devoted to calculating the transient EMP induced current on wires and cables, inside and outside the EMP source region. See, e.g., Tse Chin Mo, "EMP Generation Near Objects with Cylindrical Symmetry in the Source Region," RDA report RDA-TR-5900-002 (1974) and also DNA-3602T (June 1975); D. R. Marston, W. R. Graham, "Currents Induced in Cables in the Earth by A Continuous-Wave EM Field," (May 1966, AFWL) AFWL-EMP-3-2-#24 (1971); P. R. Barnes, "The Axial Current Induced on an Infinitely Long, Perfectly Conducting, Circular

Cylinder in Free Space by A Transient EM Plane Wave," (March 1971, AFWL) AFWL-EMP-3-4-#64 (1971); J. N. Bombardt, Jr.,"Time-Harmonic Analysis of the Induced Current on A Thin Cylinder Above A Finetely Conducting Half Space" (June 1972 , Harry Diamond Labs) AFWL-EMP-3-8-#111 (1973).

4. The ε_o and μ_o can be any constant, but their values in the vacuum are taken for all numerical evaluations. For the case of constant permeability, the $\mu = \mu_r\mu_o$ stands for both the B/H and the dB/dH--they are the same. For the case of field dependent permeability, we use $\mu = \mu_R(H)\mu_o$ to denote the differential permeability dB/dH.

5. For a previous numerical one-dimension non-linear diffussion treatment, see, e.g., E. E. Merewether, "EMP Transmission Through A Thin Sheet of Saturable Ferromagnetic Mateiral of Infinite Surface Area," IEEE, Trans. EMC, 11, 139 (Nov 1969).

6. D. G. Fink and J. M. Carroll, (editors) Standard Handbook for Electrical Engineers, 10th edition, pp 4-101 to 4-107 (McGraw-Hill, 1968). At the high frequencies and the saturating large intensities of the EMP field, the hysteresis loss is much smaller than the conductivity loss for regular iron or steel.

7. R. D. Richtmyer, K. W. Morton, Difference Method For Initial Value Problem, Chap. 8 (Interscience, 1967).

8. For a scaler field with a homogeneous boundard condition, either the field or its normal derivative, but not their mixtures, vanished on all the rod surface, and an incident plane wave not from along the semi-infinite rod, see D. S. Jones, Roy. Soc. London, 247, 449 (April 1955). Also, the hollow-pipe problem was well-known and solved,

see, e.g., D. S. Jones, The Theory of Electromagnetism, p. 594 (Pergamon, 1964); for an EMP application, see, e.g. S. W. Lee, V. Jamnejad, R. Mittra, "Near Field of Scattering by a Hollow Semi-Infinite Cylinder and Its Application to EMP sutdies," (U. of Ill. Antenna Rept., 1972) AFWL-EMP-1-13-#149 (1974); for a brief review and a recent investigation of transients from a semi-infinite cylindrical waveguide and excitations, see, e.g, N. L. Broome, "Transient Radiation From Coaxial Waveguide and Cylindrical Monopole Antennas," Ph.D. Thesis, Caltech Antenna Lab. Rept. 67 (Nov 1973).

9. A. Erdelyi (editor), Tables of Integral Transforms, Bateman Manuscript Project, Chapter 8, Volume 2, (McGraw-Hill, 1954).

10. Ref. , p. 446.

APPENDIX A. BOUNDARY CONDITIONS (7)

From the Maxwell equations, by ignoring $\varepsilon\, \partial/\partial t$ compared with σ, we have in the slab $0 < z < d$

$$\frac{\partial E}{\partial z} = -\mu_r \mu_o \frac{\partial H}{\partial t} \tag{A-1}$$

$$\sigma E = -\frac{\partial H}{\partial z} \tag{A-2}$$

which immediately give (5). Now the boundary conditions at $z = 0$ are

$$H(t,o) = H_o[f(t) + g(t)] \tag{A-3}$$

$$\frac{\partial}{\partial z} H(t,o) = -\sqrt{\frac{\mu_o}{\varepsilon_o}}\, H_o \sigma [f(t) - g(t)] \tag{A-4}$$

which immediately give (7a), and the boundary conditions at $z = d$ are

$$H(t,d) = H_o T(t) \tag{A-5}$$

$$\frac{\partial}{\partial z} H(t,d) = -\sqrt{\frac{\mu_o}{\varepsilon_o}}\, H_o \sigma T(t) \tag{A-6}$$

which immediately give (7b)

APPENDIX B. DERIVATION OF FIELDS IN THE SLAB, ONE-DIMENSIONAL PROBLEM

In the Laplace domain, (5) reads

$$\frac{\partial^2}{\partial z^2}\hat{H}(s,z) - \mu\sigma s\,\hat{H}(s,z) = 0 \tag{B-1}$$

where $H(t<0,z) \equiv 0$ has been used, and (7) reads

$$\frac{\partial}{\partial z}\hat{H}(s,o) - \sqrt{\frac{\mu_o}{\varepsilon_o}}\,\sigma\hat{H}(s,o) = -2\sqrt{\frac{\mu_o}{\varepsilon_o}}\,H_o\sigma\hat{f}(s) \tag{B-2}$$

$$\frac{\partial}{\partial z}\hat{H}(s,d) + \sqrt{\frac{\mu_o}{\varepsilon_o}}\,\sigma\hat{H}(s,d) = 0 \tag{B-3}$$

Thus, the solution of (B-1) is

$$\hat{H}(s,z) = A(s)\,e^{-\sqrt{\mu\sigma s}\,z} + B(s)\,e^{\sqrt{\mu\sigma s}\,z} \tag{B-4}$$

where A(s) and B(s) are to be determined. Now, from (B-2) we have

$$(-A + B)\sqrt{\mu\sigma s} - \sqrt{\frac{\mu_o}{\varepsilon_o}}\,\sigma(A + B) = -2\sigma\sqrt{\frac{\mu_o}{\varepsilon_o}}\,H_o\,\hat{f}(s) \tag{B-5}$$

and from (B-3) we have

$$(-A\,e^{-\sqrt{\mu\sigma s}\,d} + B\,e^{\sqrt{\mu\sigma s}\,d})\sqrt{\mu\sigma s} + \sqrt{\frac{\mu_o}{\varepsilon_o}}\,\sigma(A\,e^{-\sqrt{\mu\sigma s}\,d} + B\,e^{\sqrt{\mu\sigma s}\,d}) = 0 \tag{B-6}$$

Solving for A(s) and B(s) from (B-5) and (B-6), substituting their values into (B-4), and using (6) yields (9) and (10).

APPENDIX C. DERIVATION OF SOME APPROXIMATE FORMULAS

First, under the condition $\exp[\sqrt{\mu\sigma s}\ (z-2d)] << 1$, the magnetic field obtained by using only the A(s) term in (9a) for a δ-incidence is

$$H^{(\delta)}(t,z) \sim 2\sqrt{\frac{\sigma}{\mu_r \varepsilon_o}}\left[\frac{e^{-k^2/4t}}{\sqrt{\pi t}} - a\, e^{a^2 t + ka}\ \mathrm{erfc}\left(a\sqrt{t} + \frac{k}{2\sqrt{t}}\right)\right] \tag{C-1}$$

which reduces to (16) if $2\sigma z\sqrt{\mu_o/\varepsilon_o} >> 1$. Here $k \equiv \sqrt{\mu\sigma}\, z$ and $a \equiv \sqrt{\sigma/(\mu_r \varepsilon_o)}$.

Second, from (11') the result

$$\begin{aligned} H^{(\delta)}(t,d) &= L^{-1}\left[\frac{2\sqrt{\frac{\mu_r \varepsilon_o s}{\sigma}}}{\mathrm{Sh}(\sqrt{\mu\sigma s}\, d)}\right] \\ &= 2\sqrt{\frac{\mu_r \varepsilon_o}{\sigma}}\frac{d}{dt}\left[\frac{1}{\sqrt{\mu\sigma}\, d}\,\theta_4\left(0\,\middle|\,\frac{i\pi t}{\mu\sigma d^2}\right)\right] \\ &= 2\sqrt{\frac{\mu_r \varepsilon_o}{\sigma}}\frac{d}{dt}\left[\frac{1}{\sqrt{\mu\sigma}\, d}\sqrt{\frac{\mu\sigma d^2}{\pi t}}\sum_{-\infty}^{\infty} e^{-(n-1/2)^2 \mu\sigma d^2/t}\right] \\ &= \sqrt{\frac{\mu_r \varepsilon_o}{\sigma\pi}}\cdot\frac{1}{t^{5/2}}\sum_{1}^{\infty}\left[(2n-1)^2\mu\sigma d^2 - 2t\right] e^{\frac{-\mu\sigma d^2(2n-1)^2}{4t}} \end{aligned} \tag{C-2}$$

is used in (19)

APPENDIX D. HIGH FREQUENCY TRANSMITTED FIELD RELATIVE INCREASE

From (11'), for $\mu = \mu_>$ the ratio of the transmitted magnetic field at a frequency $s = s_>$ to that at $s = s_< < s_>$ is

$$R(\mu_>) \equiv \left(\frac{H(s_>,d)}{H(s_<,d)}\right)_{\mu_>} = \frac{(h\sqrt{\mu_> s_>})/(Sh(h\sqrt{\mu_> s_>})}{(h\sqrt{\mu_> s_<})/(Sh(h\sqrt{\mu_> s_<})} \tag{D-1}$$

where $h \equiv d\sqrt{\sigma}$. Now we want to prove that for a smaller $\mu = \mu_<$ the $R(\mu_<)$ becomes larger, i.e.

$$R(\mu_<) > R(\mu_>) \tag{D-2}$$

or rewriting it equivalently

$$\frac{Sh\ell x}{Sh(\ell r x)} > \frac{Sh\ x}{Sh(rx)} \tag{D-3}$$

Here $x \equiv h\sqrt{\mu_> s_<} > 0$, $r \equiv \sqrt{s_>/s_<} > 1$ and $\ell \equiv \sqrt{\mu_</\mu_>} < 1$. But the function $Sh(\ell x)/Sh(\ell r x)$, viewed as a function of ℓ, is monotonically decreasing since $r\ th\ y > th(ry)$ for $r > 1$ and $y > 0$. This establishes (D-3) and completes the proof.

APPENDIX E. ARGUMENT FOR EQUATION (30)

Since the slab is highly conducting with $\sigma >> \mu_r \omega \varepsilon$, whether it be saturated or not, the "amount" of field admitted into the slab is about the same for either case (see (11')). Now think of the H field as the density (one-dimensional in z) of some particles that diffuse in the slab. Then the total number of them

$$\int H dz \sim (H_{max})(\Delta z) \sim H(t_c, z_{max/t_c})\ z_{max/t_c}$$

is about the same without and with saturation, if the pulse is narrow and the slab is thick (see (28) and (29)). After t_c, both cases diffuse in the same manner and should roughly give a peak transmitted field proportional to $H(t_c, z_{max/t_c})$. This makes (30) plausible.

APPENDIX F. THE CODE DIFUSN

```
      PROGRAM DIFUSN (OUTPUT)
      DIMENSION      PSI(2,800),   A(800), X(800), Y(800)
      REAL           MUR, MU0, K
C     INCIDENT WAVE FORM AND RELATIVE PERMEABILITY FUNCTION
      S(T)=H0*SIN(W0*T)**2
      SPM(T)=H0*W0*SIN(2*W0*T)
      FMUS(H)=1.+(MUR-1)/(1.+EXP(ALPHA*(H-HCRT)))
      FMUPS(H)=1.+(MUR-1.)*EXP(-ALPHA*(H-HCRT)) /(1.+EXP(-ALPHA*(H-
     $HCRT)))
C     INCIDENT WAVE PARAMETER
      H0=1.E5
      W0=3.E9
      T0=3.1415926/W0
C     SLAB MEDIUM PARAMETER
      DSLAB=3.E-2
      MUR=1.E4
      ALPHA=2.E-2
      SIGMA=1.E7
      EPSNR=5.
C     COMPUTING PARAMETER
      HTRN=400.
      NTIME=600
      DT=T0*1.E-3
      CDT=1.02
      NZ=200
      DZ=DSLAB/NZ
C     CONSTANTS
      EPSN0=8.85E-12
      EPSN=EPSNR*EPSN0
      MU0=4*3.1415926E-7
      JU=NZ+1
      JUM1=JU-1
      JUM2=JU-2
      C1=SQRT(MU0/EPSN0)
      C2=C1*DZ
      JOUT1=1
      JOUT2=JU/6.
      JOUT3=JU*2/6.
      JOUT4=JU*3/6.
      JOUT5=JU*4/6.
      JOUT6=JU*5/6.
      JOUT7=JU
```

```
C       EXCITE THE PROGRAM
        NPROB=3
        DO 800 IPROB=1,NPROB
        IF (IPROB.EQ.1) HCRT=HTRN
        IF (IPROB.EQ.2) HCRT=4.E25
        IF (IPROB.EQ.3) HCRT=-4.E25
        PRINT 30
   30 FORMAT (* SLAB THICKNESS  PULSE WIDTH INC AMPLITUDE CRITICAL M
       < RELATIVE MU   ALPHA*,//)
        PRINT 40,DSLAB,T0,H0,HCRT,MUR,ALPHA
   40 FORMAT  (6E14.4,////)
        PRINT 50
   50 FORMAT (* TIME        H(0)        H(D/6)      H(2 D/6)    H(3 D/6)  H(
       *4 D/6)    H(5 D/6)    H(D)       ZPEAK       HMAX        ZC1         ZC2
       >  *,//)
        DO 100 JL=1,JU
  100 PSI(1,JL)=0
        T1=0
        DT=DT0
        DO 600 NL=1,NTIME
        K=1+C2*(SIGMA+EPSN/DT)
        CLL=C2*EPSN/DT
        T2=T1+DT
        DO 135  JL=2,JUM1
        IF (ALPHA*(PSI(1,JL)-HCRT),GT,300.) GO TO 130
  120 A(JL)=MU0*SIGMA*FMUR(PSI(1,JL)) *DZ**2/DT
        GO TO 135
  130 A(JL)=MU0*SIGMA*FMURS(PSI(1,JL))*DZ**2/DT
  135 CONTINUE
        X(JU)=1/K
        Y(JU)=CLL*PSI(1,JU)/K
        DO  150  IL=1,JUM2
        JL=JU-IL
        X(JL)=1/(2+A(JL)-X(JL+1))
  150 Y(JL)=X(JL)*(Y(JL+1)+A(JL)*PSI(1,JL))
        IF (T2.GE.T0)  GO TO 155
        S2=S(T2)
        SPM2=SPM(T2)
        GO TO 160
  155 S2=0
        SPM2=0
  160 CONTINUE
        SF2=2*C2*(SIGMA*S2+EPSN*SPM2)
        PSI(2,1)=(Y(2)+CLL*PSI(1,1)+SF2)/(K-X(2))
        DO  200  JL=2,JU
  200 PSI(2,JL)=X(JL)*PSI(2,JL-1)+Y(JL)
        HMAX=PSI(1,1)
        JMAX=1
```

```
      DO 225 IL=2,JU
      IF (PSI(1,IL),LE,HMAX)  GO TO 220
      HMAX=PSI(1,IL)
      JMAX=IL
  220 CONTINUE
  225 CONTINUE
      IC1=-1
      IC2=-1
      DO 240 IL=1,JU
      IF (IC1.GT.0) GO TO 230
      IF (PSI(1,IL).LT.HTRN) GO TO 240
      IC1=IL
      GO TO 240
  230 IF (PSI(1,IL).GT.HTRN)  GO TO 240
      IC2=IL
      GO TO 245
  240 CONTINUE
  245 CONTINUE
      ZC1=(IC1-1)*DZ
      ZC2=(IC2-1)*DZ
      ZPEAK=(JMAX-1)*DZ
      PRINT 250,T1, PSI(1,JOUT1),PSI(1,JOUT2),PSI(1,JOUT3),PSI(1,JOUT4),

     *PSI(1,JOUT5),PSI(1,JOUT6),PSI(1,JOUT7),ZPEAK,HMAX,ZC1,ZC2
  250 FORMAT (12E11.3)
      DO 300 JL=1,JU
  300 PSI(1,JL)=PSI(2,JL)
       T1=T2
      DT=DT*CDT
  500 CONTINUE
       PRINT 700
  700 FORMAT  (1H1)
  800 CONTINUE
      END
```

APPENDIX G. DERIVATION OF FIELDS, CYLINDRICAL PROBLEM

The ϕ-independent cylindrical TM mode in the highly conductive slab $0 < z < d$, from (35), assumes the form

$$\hat{H}_\phi = \hat{H}_\phi^{TM} = \int_0^\infty dK\, J_1(K\rho)\left[\xi(K,s)\, e^{-\sqrt{K^2+\mu\sigma s}\, z} + \eta(K,s)\, e^{\sqrt{K^2+\mu\sigma s}\, z}\right] \tag{G-1}$$

$$\hat{E}_\rho = \hat{E}_\rho^{TM} = \frac{-1}{\sigma}\frac{\partial}{\partial z}\hat{H}_\phi = \frac{-1}{\sigma}\int_0^\infty dK\sqrt{K^2+\mu\sigma s}\, J_1(K\rho)\left[-\xi(K,s)\, e^{-\sqrt{K^2+\mu\sigma s}\, z} + \eta(K,s)\, e^{\sqrt{K^2+\mu\sigma s}\, z}\right] \tag{G-2}$$

$$\hat{E}_z = \hat{E}_z^{TM} = \frac{1}{\sigma}\frac{1}{\rho}\frac{\partial}{\partial\rho}(\rho\hat{H}_\phi) = \frac{+1}{\sigma}\int_0^\infty dK\; K\, J_0(K\rho)\left[\xi(K,s)\, e^{-\sqrt{K^2+\mu\sigma s}\, z} + \eta(K,s)\, e^{\sqrt{K^2+\mu\sigma s}\, z}\right] \tag{G-3}$$

where the finiteness of the fields at $\rho = 0$ has been used to choose the Bessel function of first kind. Similarly, the fields in $z > d$ can be expressed as

$$\hat{E}_z = \hat{E}_z^{TM} = \left(\frac{\partial^2}{\partial z^2} - s^2\mu_o\varepsilon_o\right)\hat{V}(s,\rho,z)$$

$$= \left(\frac{\partial^2}{\partial z^2} - s^2\mu_o\varepsilon_o\right)\int_0^\infty dK \cdot p(K,s)\, J_o(K\rho)\, e^{-\sqrt{K^2+\mu_o\varepsilon_o s^2}\,(z-d)}$$

$$= \int_0^\infty dK \cdot K^2 \, p(K,s) \, J_o(K\rho) \, e^{-\sqrt{K^2+\mu_o\varepsilon_o s^2}\,(z-d)} \qquad \text{(G-4)}$$

$$\hat{H}_\phi = \hat{H}_\phi^{TM} = - s\varepsilon_o \frac{\partial}{\partial \rho} \hat{V}(s,\rho,z)$$

$$= s\varepsilon_o \int_0^\infty dK \cdot K \, p(K,s) \, J_1(K\rho) \, e^{-\sqrt{K^2+\mu_o\varepsilon_o s^2}\,(z-d)}$$

(G-5)

$$\hat{E}_\rho = \hat{E}_\rho^{TM} = \frac{\partial^2}{\partial \rho \partial z} \hat{V}(s,\rho,z)$$

$$= \int_0^\infty dK \cdot K\sqrt{K^2 + \mu_o\varepsilon_o s^2} \, p(K,s) \, J_1(K\rho) \, e^{-\sqrt{K^2+\mu_o\varepsilon_o s^2}\,(z-d)}$$

(G-6)

where the $\hat{V}(s,\rho,z)$ is the cylindrical TM Hertz potential, and the requirement that the wave be positive-z traveling has been used to choose the negative exponential expression. In the above, the choices of branch cuts (as a function of s) are such that

$$\text{Real } \{\sqrt{k^2 + \mu\sigma s}\} > 0 \qquad \text{(G-7)}$$

$$\text{Real } \{\sqrt{k^2 + \mu_o\varepsilon_o s^2}\} > 0 \qquad \text{(G-8)}$$

Now at $z = d$, the continuity of H_ϕ gives

$$\xi(K,s)\ e^{-K_> d} + \eta(K,s)\ e^{K_> d} = s\varepsilon_o K\ p(K,s) \qquad \text{(G-9)}$$

and the continuity of E_ρ gives

$$\frac{-K_>}{\sigma}\left[-\xi(K,s)\ e^{-K_> d} + \eta(K,s)\ e^{K_> d}\right] = KK_<\ p(K,s) \qquad \text{(G-10)}$$

where $K_> \equiv \sqrt{K^2+\mu\sigma s}$ and $K_< \equiv \sqrt{K^2+\mu_o\varepsilon_o s^2}$. At $z = 0$, requiring that the total magnetic field be the approximate value (34) and using the integration expression

$$\int_0^\infty dK\ J_1(K\rho)\ J_o(Ka) = \frac{1}{\rho}\ , \quad \rho > a \qquad \text{(G-11)}$$

$$= 0\ , \quad \rho < a \qquad \text{(G-12)}$$

gives

$$\xi(K,s) + \eta(K,s) = \frac{I_o}{2\pi} J_o(Ka) \cdot \frac{2\hat{f}(s)\left[(1+\alpha) - (1-\alpha)\ e^{-2\sqrt{\mu\sigma s}\ d}\right]}{(1+\alpha)^2 - (1-\alpha)^2\ e^{-2\sqrt{\mu\sigma s}\ d}}$$

$$\equiv q(K,s) \qquad \text{(G-13)}$$

Solving (G-9), (G-10) and (G-13) gives

$$\begin{pmatrix}\xi(K,s)\\ \eta(K,s)\end{pmatrix} = \frac{\begin{pmatrix}(1+\beta)\ e^{K_> d}\\ -(1-\beta)\ e^{-K_> d}\end{pmatrix} q(K,s)}{e^{K_> d}(1-\beta) - e^{-K_> d}(1-\beta)} \qquad \text{(G-14)}$$

$$p(K,s) = \frac{q(K,s)}{s\varepsilon_o K} \cdot \frac{2\beta}{e^{K_> d}(1+\beta) - e_1^{-K_> d}(1-\beta)} \qquad \text{(G-15)}$$

where $\beta \equiv s\varepsilon_o K_> / (\sigma K_<)$. These give (38), (39) and (41).

If $\alpha \equiv (\mu_r \varepsilon_o s/\sigma)^{1/2} << 1$, thus $\beta << 1$, and $\sigma d \sqrt{\mu_o/\varepsilon_o} >> 1$, a practical condition as stated in (23) which implies

$$\frac{\alpha\ Ch(\sqrt{\mu\sigma d}\ s)}{Sh(\sqrt{\mu\sigma d}\ s)} << 1 \qquad \text{(G-16)}$$

and

$$\frac{\beta\ Ch(K_> d)}{Sh(K_> d)} << 1 \qquad \text{(G-17)}$$

then ξ, η, and p are simplified to

$$\begin{pmatrix} \xi(K,s) \\ \eta(K,s) \end{pmatrix} = \begin{pmatrix} (1+\beta)\ e^{K_> d} \\ -(1-\beta)\ e^{-K_> d} \end{pmatrix} \frac{\lambda(K,s)}{2Sh(K_> d)} \cdot \left[1 - \frac{\alpha Ch(\sqrt{\mu\sigma s}\ d)}{Sh(\sqrt{\mu\sigma z}\ d)} - \frac{\beta Ch(K_> d)}{Sh(K_> d)}\right]$$

$$= \frac{\lambda(K,s)}{2Sh(K_> d)} \begin{pmatrix} e^{K_> d}\left[1 + \beta - \frac{\beta Ch(K_> d)}{Sh(K_> d)} - \frac{\alpha Ch(\sqrt{\mu\sigma s}\ d)}{Sh(\sqrt{\mu\sigma s}\ d)}\right] \\ -e^{K_> d}\left[1 - \beta - \frac{\beta Ch(K_> d)}{Sh(K_> d)} - \frac{\alpha Ch(\sqrt{\mu\sigma s}\ d)}{Sh(\sqrt{\mu\sigma s}\ d)}\right] \end{pmatrix} \qquad \text{(G-18)}$$

$$p(K,s) = \frac{\lambda(K,s) K_>}{\sigma K K_< Sh(K_> d)} \cdot \left[1 - \frac{\alpha Ch(\sqrt{\mu\sigma s}\ d)}{Sh(\sqrt{\mu\sigma s}\ d)} - \frac{\beta Ch(K_> d)}{Sh(K_> d)}\right] \qquad \text{(G-19)}$$

where

$$\lambda(K,s) \equiv \frac{I_o J_o(Ka)\ \hat{f}(s)}{\pi} \qquad \text{(G-20)}$$

These give (42) and (43).

APPENDIX H. APPROXIMATE EXPRESSIONS FOR CYLINDRICAL PROBLEM

From (40b) and (43), we have

$$E_\rho(t,\rho,d) \sim L^{-1} \int_0^\infty dK\, J_1(K\rho)\, J_o(Ka)\, \frac{I_o}{2\pi} \cdot \frac{2\hat{f}(s)}{\sigma} \quad \frac{K_>}{Sh\ K_>d}$$

$$= \frac{I_o}{\pi\sigma} \int_0^\infty dK\, J_1(K\rho)\, J_o(Ka)\, L^{-1}\, \frac{\hat{f}(s)K_>}{Sh\ K_>d}$$

$$= \frac{I_o}{\pi\sigma d} \int_0^\infty dK\, J_1(K\rho)\, J_o(Ka) \int_0^t dt'\, f(t-t')\, e^{(-K^2t')/(\mu\sigma)}$$

$$\left[\frac{d}{dt'}\, \theta_4\left(0 \middle| \frac{i\pi t'}{\mu\sigma d^2}\right)\right]$$

$$= \frac{I_o}{\pi\sigma d} \int_0^t dt'\, f(t-t')\left[\frac{d}{dt'}\, \theta_4\left(0 \middle| \frac{i\pi t'}{\mu\sigma d^2}\right)\right]$$

$$\int_0^\infty dK\, J_1(K\rho)\, J_o(Ka)\, e^{(-K^2t')/(\mu\sigma)} \qquad \text{(H-1)}$$

$$\sim \frac{I_o}{\pi\sigma d} \int_0^\infty dt'\, f(t-t')\left[\frac{d}{dt'}\, \theta_4\left(0 \middle| \frac{i\pi t'}{\mu\sigma d^2}\right)\right] \cdot \frac{1 - e^{(-\rho^2\mu\sigma/4t')}}{\rho}$$

$$\text{if } \rho >> \min\left(a, \sqrt{\frac{t'}{\mu\sigma}}\right) \qquad \text{(H-2)}$$

$$\sim \frac{I_o}{\pi\sigma d} \int_0^\infty dt'\, f(t-t')\left[\frac{d}{dt'}\, \theta_4\left(0 \middle| \frac{i\pi t'}{\mu\sigma d^2}\right)\right] \cdot \frac{\mu\sigma\rho}{4t'} \cdot e^{(-a^2\mu\sigma/4t')}$$

$$\text{if } \rho << \max\left(a, \sqrt{\frac{t'}{\mu\sigma}}\right) \qquad \text{(H-3)}$$

Thus the δ-response for an incident $H^{inc} = a\,\delta(t - z/c)/\rho$, i.e., $H_o f(t) = \delta(t)$, is

$$E_\rho^{(\delta)}(t,\rho,d) = \frac{2a}{\sigma d}\left[\frac{d}{dt}\,\theta_4\left(0\middle|\frac{i\pi t}{\mu\sigma d^2}\right)\right]\int_0^\infty dK\, J_1(K\rho)\, J_o(Ka)\, e^{(-K^2 t)/(\mu\sigma)}$$

(H-4)

$$\sim \frac{2a}{\sigma d}\left[\frac{d}{dt}\,\theta_4\left(0\middle|\frac{i\pi t}{\mu\sigma d^2}\right)\right]\cdot\frac{1 - e^{(-\mu\sigma\rho^2)/(4t)}}{\rho}$$

$$\text{if } \rho >> \min\left(a, \sqrt{\frac{t}{\mu\sigma}}\right) \tag{H-5}$$

$$\sim -\frac{2a}{\sigma d}\left[\frac{d}{dt}\,\theta_4\left(0\middle|\frac{i\pi t}{\mu\sigma d^2}\right)\right]\cdot\frac{\mu\sigma\rho}{4t}\, e^{(-\mu\sigma a^2)/(4t)}$$

$$\text{if } \rho << \max\left(a, \sqrt{\frac{t}{\mu\sigma}}\right) \tag{H-6}$$

Similarly, from (40a) and (43), we have

$$H_\phi(t,\rho,d) = L^{-1}\int_0^\infty dK\, J_1(K\rho)\, J_o(Ka)\,\frac{s\varepsilon_o I_o}{\pi\sigma}\cdot\frac{\hat{f}(s)\,K_>}{K_< Sh(K_> d)}$$

$$= L^{-1}\int_0^\infty dK\, J_1(K\rho)\,\tilde{\hat{E}}_\rho(s,K,d)\,\frac{s\varepsilon_o}{K_<}$$

$$= \int_0^\infty dK\, J_1(K\rho)\,\varepsilon_o\, L^{-1}\left(\tilde{\hat{E}}_\rho(s,K,s)\,\frac{s}{K_<}\right)$$

$$= \int_0^\infty dK\, J_1(K\rho)\, \varepsilon_o \cdot \left[\tilde{E}_\rho(t,k,d) * \left[\frac{d}{dt} L^{-1}\left(\frac{1}{K_<}\right) + \left(L^{-1}\left(\frac{1}{K_<}\right)\right)_{t=0} \delta(t) \right] \right]$$

$$= \int_0^\infty dK\, J_1(K\rho)\, \varepsilon_o \cdot \left[\tilde{E}_\rho(t,K,d) \right.$$

$$\left. * \left[\delta(t) - \frac{K}{\sqrt{\mu_o \varepsilon_o}} J_1\left(\frac{Kt}{\sqrt{\mu_o \varepsilon_o}}\right) \right] \frac{1}{\sqrt{\mu_o \varepsilon_o}} \right]$$

$$= \sqrt{\frac{\varepsilon_o}{\mu_o}} \left[E_\rho(t,\rho,d) - \int_0^\infty dK\, J_1(K\rho) \int_0^t dt' \frac{K}{\sqrt{\mu_o \varepsilon_o}} \right.$$

$$\left. J_1\left(\frac{Kt'}{\sqrt{\mu_o \varepsilon_o}}\right) \tilde{E}_\rho(t - t',K,d) \right]$$

$$= \sqrt{\frac{\varepsilon_o}{\mu_o}} \left[E_\rho(t,\rho,d) - \int_0^\infty dK\, J_1(K\rho) \int_0^t dt' \frac{K}{\sqrt{\mu_o \varepsilon_o}} \right.$$

$$J_1\left(\frac{Kt'}{\sqrt{\mu_o \varepsilon_o}}\right) \frac{I_o}{\pi \sigma d} J_o(Ka) \int_0^{t-t'} dt''\, f(t-t'-t'')\, e^{(-K^2 t'')/(\mu\sigma)}$$

$$\left. \left[\frac{d}{dt''} \theta_4\left(0 \middle| \frac{i\pi t''}{\mu \sigma d^2}\right) \right] \right]$$

$$= \sqrt{\frac{\varepsilon_o}{\mu_o}} \left[E_\rho(t,\rho,d) - \frac{I_o}{\sigma \pi d \sqrt{\mu_o \varepsilon_o}} \int_0^t dt' \int_0^{t-t'} dt''\, f(t-t'-t'') \right.$$

$$\left. \left[\frac{d}{dt''} \theta_4\left(0 \middle| \frac{i\pi t''}{\mu \sigma d^2}\right) \right] \int_0^\infty dK\, K J_1\left(\frac{Kt'}{\sqrt{\mu_o \varepsilon_o}}\right) J_o(Ka)\, J_1(K\rho)\, e^{(-K^2 t'')/(\mu\sigma)} \right]$$

$$= \sqrt{\frac{\varepsilon_o}{\mu_o}} \left[E_\rho(t,\rho,d) - \frac{I_o}{\pi\sigma d \sqrt{\mu_o \varepsilon_o}} \int_0^t dt'' \left[\frac{d}{dt''} \theta_4\left(0 \middle| \frac{i\pi t''}{\mu\sigma d^2}\right)\right] \right.$$

$$\int_0^{t-t''} dt' \; f(t-t'-t'') \int_0^\infty dK \; K J_1\left(\frac{Kt'}{\sqrt{\mu_o \varepsilon_o}}\right) J_o(Ka) \; J_1(K\rho)$$

$$\left. e^{(-K^2 t'')/(\mu\sigma)} \right]$$

$$= \sqrt{\frac{\varepsilon_o}{\mu_o}} \; E_\rho(t,\rho,d) + H_{\phi,dev}(t,\rho,d) \qquad \text{(H-7)}$$

from which

$$H_{\phi,dev}(t,\rho,d) \sim \frac{-I_o}{\mu\sigma d \mu_o} \int_0^t dt'' \int_0^{t-t''} dt' \; f(t-t'-t'') \left[\frac{d}{dt''} \theta_4\left(0 \middle| \frac{i\pi t''}{\mu\sigma d^2}\right)\right]$$

$$\cdot \frac{\mu\sigma}{2t''} \; e^{[\mu\sigma(\rho^2 + c^2 t'^2)]/(-4t'')} \; I_1\left(\frac{\mu\sigma c\rho t'}{2t''}\right)$$

$$\text{if } a << \max\left(\rho, \frac{t'}{\sqrt{\mu_o \varepsilon_o}}\right) \qquad \text{(H-8)}$$

$$\sim \frac{-I_o}{\pi\sigma d \mu_o} \int_0^t dt'' \int_0^{t-t''} dt' \; f(t-t'-t'') \left[\frac{d}{dt''} \theta_4\left(0 \middle| \frac{i\pi t''}{\mu\sigma d^2}\right)\right]$$

$$\cdot \frac{\rho t'}{4\sqrt{\mu_o \varepsilon_o}} \left(\frac{\mu\sigma}{2t''}\right)^3 \; e^{(-\mu\sigma a^2)/(4t'')} \left(\frac{4t''}{\mu\sigma} - a^2\right)$$

$$\text{if } a >> \max\left(\rho, \frac{t'}{\sqrt{\mu_o \varepsilon_o}}\right) \qquad \text{(H-9)}$$

Thus, the δ-response for a $H^{inc} = a\,\delta(t - \frac{z}{c})/\rho$ is

$$H^{(\delta)}_{\phi,dev}(t,\rho,d) = -\frac{2\,a}{\sigma d\mu_o}\int_0^t dt''\left[\frac{d}{dt''}\,\theta_4\left(0\middle|\frac{i\pi t''}{\mu\sigma_d{}^2}\right)\right]$$

$$\int_0^\infty dK\; KJ_1\left(\frac{K(t-t'')}{\sqrt{\mu_o\varepsilon_o}}\right)\; J_o(Ka)\; J_1(K\rho)\; e^{(-K^2t'')/(\mu\sigma)}$$

(H-10)

In particular, if $a << \max\left(\rho, \frac{t-t''}{\sqrt{\mu_o\varepsilon_o}}\right)$ it becomes

$$H^{(\delta)}_{\phi,dev}(t,\rho,d) \sim \frac{-2\,a}{\sigma d\mu_o}\int_0^t dt''\left[\frac{d}{dt''}\,\theta_4\left(0\middle|\frac{i\pi t''}{\mu\sigma d^2}\right)\right]\frac{\mu\sigma}{2t''}$$

$$e^{[\mu\sigma(\rho^2+c^2(t-t'')^2)]/(-4t'')}\; I_1\left(\frac{\mu\sigma c\rho\,(t-t'')}{-2t''}\right)$$

$$\sim \frac{-2\,a}{\sigma d\mu_o}\left[\frac{d}{dt}\,\theta_4\left(0\middle|\frac{i\pi t}{\mu\sigma d^2}\right)\right]\frac{\mu\sigma}{2t}\,\frac{\mu\sigma c\rho}{4t}\int_0^t dt''(t-t'')$$

$$e^{[\mu\sigma(\rho^2+c^2(t-t'')^2)]/(-4t)}$$

$$\sim \frac{-2a\mu^2\sigma c\rho}{8\mu_o\sigma dt^2}\left[\frac{d}{dt}\,\theta_4\left(0\middle|\frac{i\pi t}{\mu\sigma d^2}\right)\right]\; e^{(-\mu\sigma\rho^2)/(4t)}$$

$$\int_0^\infty d\tau\;\tau e^{(-\mu\sigma c^2\tau^2)/(4t)}$$

$$= -\sqrt{\frac{\varepsilon_o}{\mu_o}}\,\frac{2a}{\sigma d}\left[\frac{d}{dt}\,\theta_4\left(0\middle|\frac{i\pi t}{\mu\sigma d^2}\right)\right]\,e^{(-\mu\sigma\rho^2)/(4t)}\,\frac{\mu\sigma\rho}{4t}$$

(H-11)

Here a condition on the time

$$e^{(\mu\sigma c^2 t)/4} \gg 1 \tag{H-12}$$

has been used to validate the third equality in (H-11). For cases of practical interest, (H-12) is amply satisfied for times up to the peak diffusion time $t_{pk/d} \sim 10^{-1}\,\mu\sigma d^2$ at $z = d$, because usually we have

$$\frac{0.1}{4}\,(\mu\sigma cd)^2 \gg 1 \leftrightarrow 1.4 \times 10^{12} \times \left(\mu_1 \times \frac{\sigma}{2\times10^7} \times \frac{d}{10^{-3}}\right)^2 \gg 1$$

(H-13)

On the other hand, if $a \gg \rho$ the $H^{(\delta)}_{\phi,dev}$ becomes

$$H^{(\delta)}_{\phi,dev}(t,\rho,d) \sim \frac{-2a}{\sigma d\mu_o}\int_0^t dt''\left[\frac{d}{dt''}\,\theta_4\left(0\middle|\frac{i\pi t''}{\mu\sigma d^2}\right)\right]\left(\frac{-\rho}{2c}\right)$$

$$\frac{\partial}{\partial t}\left[\frac{\mu\sigma}{2t''}\,e^{\mu\sigma(a^2+c^2(t-t'')^2)/(-4t'')}\,I_o\left(\frac{\mu\sigma ac(t-t'')}{2t''}\right)\right]$$

$$\sim \sqrt{\frac{\varepsilon_o}{\mu_o}}\,\frac{2a}{\sigma d}\left[\frac{d}{dt}\,\theta_4\left(0\middle|\frac{i\pi t}{\mu\sigma d^2}\right)\right]\,e^{(-\mu\sigma a^2)/(4t)}\,\frac{\mu\sigma\rho}{4t}\cdot\frac{\mu\sigma a^2}{4t}$$

(H-14)